Geophysical Journal International

Site-city interaction: theoretical, numerical and experimental crossed-analysis

L. Schwan,[1] C. Boutin,[2] L.A. Padrón,[3] M.S. Dietz,[4] P.-Y. Bard[5] and C. Taylor[4]

[1]*Acoustics Research Centre, University of Salford, Newton Building, Salford* M5 4WT*, United Kingdom. E-mail:* logan.schwan@gmail.com
[2]*ENTPE/LGCB, CNRS UMR 5513, CeLyA, Université de Lyon, Rue Maurice Audin,* 69518 *Vaulx-en-Velin cedex, France*
[3]*University Institute SIANI, Universidad de Las Palmas de Gran Canaria, Las Palmas, Spain*
[4]*BLADE, Department of Civil Engineering, University of Bristol, Queen's Building, University Walk, Clifton BS8 1TR, United Kingdom*
[5]*ISTerre/IFSTTAR, CNRS UMR* 5275*, Université de Grenoble, BP* 53*, F-*38041 *Grenoble Cedex 9, France*

SUMMARY

The collective excitation of city structures by a seismic wavefield and the subsequent multiple Structure-Soil-Structure Interactions (SSSIs) between the buildings are usually disregarded in conventional seismology and earthquake engineering practice. The objective here is to qualify and quantify these complex multiple SSSIs through the design of an elementary study case, which serves as a benchmark for theoretical, numerical and experimental crossed-analysis. The experimental specimen consists of an idealized site-city setup with up to 37 anisotropic resonant structures arranged at the top surface of an elastic layer and in co-resonance with it. The experimental data from shaking table measurements is compared with the theoretical and numerical results provided respectively by an equivalent city-impedance model derived analytically from homogenization in the long-wavelength approximation and a model based on boundary elements. The signatures of the site-city interactions are identified in the frequency, time and space domain, and in particular consist of a frequency-dependent free/rigid switch in the surface condition at the city resonance, beatings in the records and the depolarization of the wavefield. A parametric study on the city density shows that multiple SSSIs among the city structures (five are sufficient) can have significant effects on both the seismic response of its implantation site and that of the buildings. Key parameters are provided to assess site-city interactions in the low seismic frequency range: They involve the mass and rigidity of the city compared to those of the soil and the damping of the building.

Key words: Earthquake dynamics; Earthquake ground motions; Body waves; Seismic anisotropy; Site effects; Wave propagation.

1 INTRODUCTION

Urban and industrial areas require a particular attention in seismic analysis due to the concentrations of population, real estates, strategic public services and human activities having a large socioeconomical impact. However, the presence of the city is usually disregarded in conventional methods applied in seismology and earthquake engineering: The ground motion is supposed to result from the seismic source and substratum properties only, for example, Bonnefoy-Claudet *et al.* (2008), while the response of a structure to the ground motion is studied independently from the surrounding buildings, for example, Jennings & Bielak (1973). These standard approaches omit the effects of multiple soil-structures dynamic interactions on the seismic field and the buildings' response.

While these approximations are reasonable in most cases, they are questionable in urban areas, where high-rise buildings, similar in height and design, are built closely from one another. Neighbouring buildings can exchange significant amounts of energy with each other, and form, with the soil, a fully coupled dynamic system that should be treated as a whole. The problem of mutual interactions between two buildings have been formulated initially by Luco & Contesse (1973) and extended to that of multiple interactions among a group of buildings by Wong & Trifunac (1975). Later, Wirgin & Bard (1996) suggested that such collective interactions among buildings of a city, the so-called 'site-city interaction', could provide a possible explanation for atypical features observed in accelerograms from the 1985 Michoacan earthquake: Some records in Mexico City exhibited long durations and beatings (Singh & Ordaz 1993) which could not find a satisfying explanation through geological site-effects only (Chávez-García & Bard 1994). In fact, Mexico is favourable to site-city interactions: The

clay softness favours soil-structure interactions, and the natural frequencies of buildings are close to the basin's one, thus magnifying energy exchanges.

The idea of site-city interactions has been supported by different numerical simulations based on various methods (finite/boundary elements methods, Green functions, etc.) and performed on simplified cities (2-D or 3-D, periodic or random arrangements) or on groups of nearby buildings (Clouteau & Aubry 2001; Guéguen *et al.* 2002; Tsogka & Wirgin 2003; Groby *et al.* 2005; Kham *et al.* 2006; Ghergu & Ionescu 2009; Padrón *et al.* 2009). As the capacities of computers increase, more and more complex situations can be studied. For instance, the numerical simulations of Taborda & Bielak (2011) and Isbiliroglu *et al.* (2015) have been conducted on a supercomputer having 480 processors (Taborda & Bielak 2011), with simulations running for up to 15 hours (Isbiliroglu *et al.* 2015) in order to compute the response of up to 81 building-like homogeneous blocks arranged at the surface of a realistic geologic stratification, when submitted to the ground motion recorded during the 1994 Northridge earthquake.

All these simulations tend to corroborate the idea that the city can interact as a whole with its site, especially at the buildings resonance. In-situ measurements on single structures already showed that buildings can irradiate significant energy in the soil (Jennings 1970; Chávez-García & Cárdenas-Soto 2002; Castellaro & Mulargia 2010). Besides, experiments on small-scale specimens consisting of a limited number of closed-spaced buildings (less than 5) have also been performed on shaking table (Kitada *et al.* 1999) or in centrifuge (Chazelas *et al.* 2003) and showed that (multiple) soil-structure interactions can have noticeable effects on the dynamic response of the structures and ground motion. The same trend is observed with the alternative approach developed by Boutin & Roussillon (2004, 2006) to derive analytically the effective behaviour of idealized city arrangements: Provided that the representative surface element of the city (constituted by one or few buildings) is much smaller than the seismic wavelength, the homogenization of periodic systems (Sánchez-Palencia 1980; Auriault *et al.* 2009) enables to describe the city as a surface impedance that modifies the usual condition of free field (Schwan & Boutin 2013; Boutin *et al.* 2015).

Despite these convergent observations, it is still uncertain in practice whether a city group-effect can noticeably modify the seismic response of its implantation site and constitutive buildings. In particular, the extent up to which the conventional approaches remain efficient is still an open question. This uncertainty may rely on the three following facts. First, the identification of a possible 'site-city' effect in the records obtained during earthquake events is a very hard task, due to the specificity of each site-city configuration and to the huge amount of information required to discriminate that effect from other complex phenomena. Second, the basic experimental data that would clearly evidence a 'site-city' effect is missing: Too few accelerograms are gained during earthquake events (compared to the complexity of the geological site and the city) and, up-to-date, no experiments dealing with multistructure interactions among a large group of buildings (say more than 10) have been performed. Third, it is difficult to draw general conclusions or physical rules from the several numerical approaches mentioned above, due to the vast variety of assumptions retained for the building models (single or multiple degrees of freedom), the city model (geometric arrangement, buildings with similar or distinct masses, stiffness, eigenfrequencies), the frequency range of investigation (compared to the buildings and site eigenfrequencies), the nature of the incident wave, and the 2-D or 3-D character of the numerical simulation. Further, the different methodologies required by each method makes uneasy (if not impossible) a reliable comparison of the results, expressed in the time or frequency domain, in acceleration or displacement, etc.

Motivated by the above observations, a study case is developed that favours experimental, numerical and theoretical crossed-analyses and enables to improve the physical insight into this complex phenomenon. The multiple SSSIs are investigated through an idealized experimental setup and the resulting data is compared with two models: the theoretical city-impedance model (CIM) derived from homogenization (Boutin & Roussillon 2004, 2006); and a numerical model consisting of a Boundary Elements (BE) approach (Padrón *et al.* 2004). This paper is organized as follows: The methodology is presented in Section 2; the CIM is described in Sections 3 and 4; the experimental set-up is designed in Section 5 and the numerical model in Section 6; the experimental results are presented and compared to the theoretical and numerical models in Section 7. The main outcomes are discussed in the Conclusion.

2 CROSSED-ANALYSIS METHODOLOGY

Idealization of urban landscapes. With the development of Geographic Information Systems and imaging networks such as satellite (Sohn & Dowman 2007) or aerial imaging (Adeline *et al.* 2013), urban morphology can be characterized over large areas, Fig. 1. While shapes, sizes and densities of buildings seem to be characteristics of socioeconomic blocks, for example, residential, commercial or business districts (Yoshida & Omae 2005), a city-taxonomy has been proposed by Figueiredo & Amorim (2007) based upon the likeness of urban arrangements to a grid. Those observations suggest the possibility to idealize some city districts as the periodic distribution of similar structures. The present study focuses especially on those made of high(-rise) heavy multistorey buildings capable of strong soil/structure interactions, and the fundamental resonance of which occur within the seismic frequency range. Examples of idealized city districts are shown in Figs 2(a) and (b) for isotropic (same resonant behaviour in both principal horizontal directions) and anisotropic buildings respectively. They consist of the Σ-periodic arrangement of linear resonant structures at the top plane surface Γ (outward normal **n**) of a homogeneous (near-)elastic linear isotropic layer, with elastic tensor **C**, shear modulus μ, Poisson's ratio ν, weak damping $\xi_s \ll 1$ and density ρ.

Equivalent CIM. The propagation of small elastic perturbations is investigated in such idealized systems. The study is performed in the harmonic regime at the frequency $f = \omega/2\pi$ close to the eigenfrequency $\omega_o/2\pi$ of the resonant structures. In that frequency range, a scale
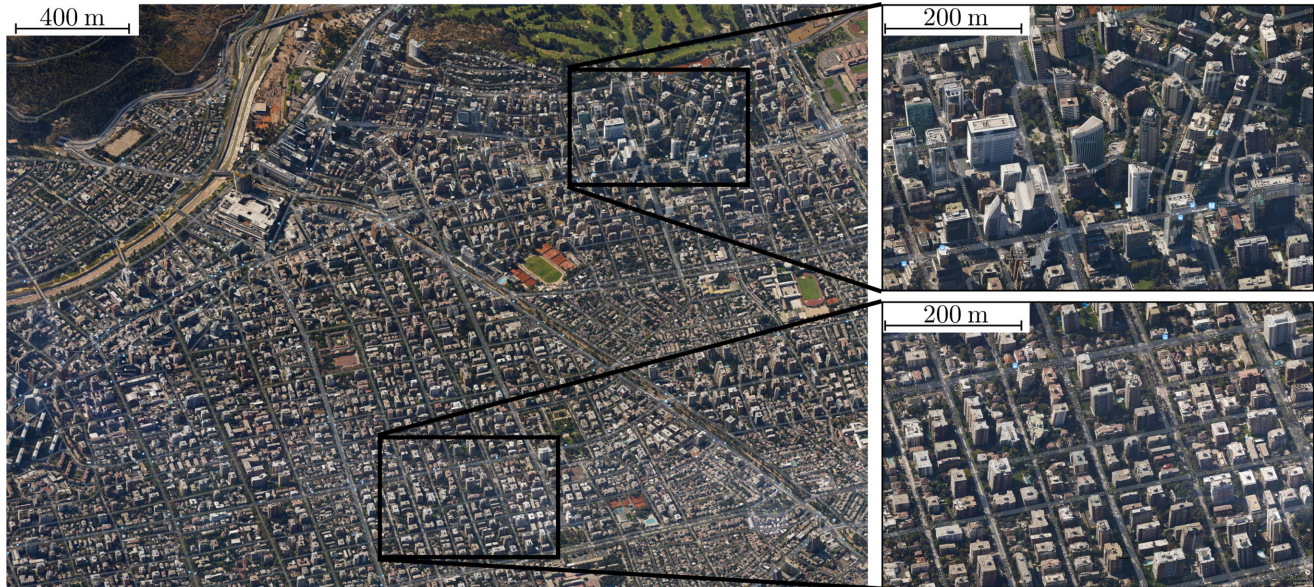
Figure 1. An example of urban landscape. Satellite view of San Cristobal district, Santiago de Chile, Chile. Coordinates in the World Geodetic System 84 in decimal degrees: latitude $= [-33.435; -33.409]$ and longitude $= [-70.616; -70.584]$. On the right: zooms at grid-like arrangements of similar structures. Source: Google Maps, available at https://maps.google.fr/ (last accessed in March 2015).
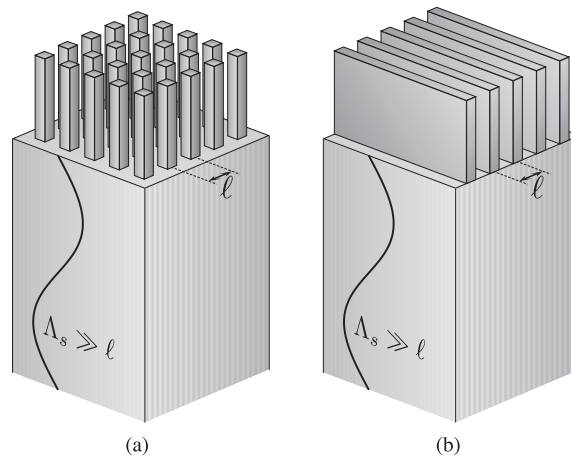

Figure 2. Idealization of urban landscapes: (a) isotropic buildings; (b) anisotropic buildings. Illustration of the scale separation: the seismic wavelength Λ_s is much larger than the size ℓ of the period Σ.

separation is assumed whereby the characteristic size ℓ of the period Σ is much smaller than the reduced shear wavelength $\Lambda_s = c_s/f = 2\pi/k$ in the medium, where $c_s = \sqrt{\mu/\rho}$ is the shear wave speed and k the wavenumber. This scale separation is quantified by the following scale parameter:

$$\varepsilon = 2\pi\ell/\Lambda_s = k\ell \ll 1. \tag{1}$$

The smallness of $\varepsilon \ll 1$ along with the periodic distribution of structures enables the formulation of the elastodynamic problem within the usual framework of two-scale asymptotic homogenization (Sánchez-Palencia 1980; Auriault *et al.* 2009). The theoretical analysis, presented in Sections 3 and 4 and developed in Appendix, has been initially proposed by Boutin & Roussillon (2006). It relies on the localization within a boundary layer of the near-fields scattered by the city, and leads to reduce the resonant array of buildings into an equivalent surface impedance. Arising from the building/city up-scaling, this city-impedance inherits frequency-dependence and anisotropic behaviours from the buildings, and induces unconventional reflection properties such as directional free/rigid switches in the boundary conditions, atypical depolarization effects (Boutin *et al.* 2015) and unusual mode conversions (Schwan & Boutin 2013). When the assumptions are fulfilled, this approach provides a simple analytical expression for 3-D formulation of the site-city effect, well-adapted for parametric studies and design.

Site-city setup. A site-city setup is devised from the city-impedance analysis in order to enclose the singular predictions made by that model (Section 5). The setup is realized with up to 37 anisotropic resonators and tested on a large shaking table (3 m wide platform with 21 ton payload). The properties of the experimental model (about 4 m^3) are scaled to suit the capabilities of the shaking table (optimized in the frequency range 0.5–25 Hz).
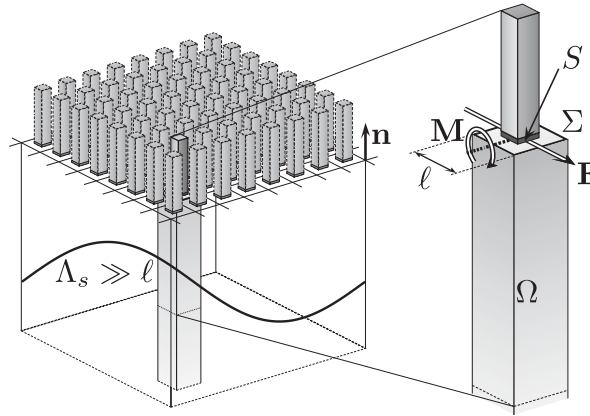
Figure 3. Illustration of the two-scale physics in the system in the case of a single isotropic structure on each period Σ. On the long-wavelength scale (left): propagation of the seismic field in the presence of the periodic arrangement of structure. On the local scale (right): the building applies the force **F** and moment **M** on its rigid foundation S. Representation of the volume Ω of integration for the local problem.

Numerical modelling. Independently from the CIM, the site-city setup is analysed as a study case using a 2-D numerical model based on BE (Padrón *et al.* 2004) to solve the elastodynamic problem for the soil together with the dynamic response of the buildings, see Section 6. Using the same fundamental equations and basic assumptions as the CIM, the numerical analysis disregards none of the phenomena that have been left aside as correctors in the asymptotic approach of homogenization. Moreover, the numerical model does not depend on the scale separation and it accounts for the finite extent of the setup. As a counterpart, the numerical procedure only applies in 2-D, results require heavy computations, and the specific physics underlying the phenomena is not condensed in a simple closed-form expression.

Crossed-analysis and discussion. Both CIM and BE model (BEM) are applied to the site-city setup and their results are compared to experimental data in Section 7. The objectives are (1) to evidence the unconventional phenomena predicted by the CIM, (2) to demonstrate the agreement (qualitative and quantitative) between the predictions and the experimental results, especially regarding the atypical phenomena and (3) to compare the models with one another.

3 MULTISCALE ANALYSIS

The homogenization of the idealized Σ-periodic city in an equivalent impedance is presented in this section. The model of Boutin & Roussillon (2006) is applied and extended here to slender resonant structures settled on rigid foundations adhered to the elastic (or viscoelastic) half-space. For clarity, only one structure is considered on each period Σ, for example, Fig. 3, but the case of multiple structures on each period Σ would follow the same procedure.

3.1 Homogenization method

Following the method described by Sánchez-Palencia (1980), the homogenization of the city is based on two main steps: The two-scale description of space and the asymptotic expansion of the fields.

Two-scale description of space. The scale separation in eq. (1) introduces two characteristic lengths in the system: The macroscopic size $L = \Lambda_s/2\pi$ of the seismic field and the lattice size $\ell = \mathcal{O}(\varepsilon L)$ of the city arrangement. To describe field variations at both scales, two space-variables are used, linked by the scale ratio ε: The macrovariable **x** and the microvariable $\mathbf{y} = \varepsilon^{-1}\mathbf{x}$. The differentiation of the fields is modified using both space variables **x** and **y**; for instance $\mathbf{grad} = \mathbf{grad_x} + \varepsilon^{-1}\mathbf{grad_y}$ where $\mathbf{grad_x}$ and $\mathbf{grad_y}$ denote the gradients with respect to **x** and **y**. The space-variables are defined in the Cartesian coordinate system $(\mathbf{e}_1, \mathbf{e}_2, \mathbf{e}_3)$ with $\mathbf{e}_3 = \mathbf{n}$ as the outward normal. In the local description, that is, with the microvariable **y**, the origin O of the local frame is chosen at the centre of the period Σ.

Asymptotic expansions. The physical fields (motion and stress) are expanded asymptotically in powers of ε. The expansions are substituted in the elastodynamic equations (elastic constitutive law and dynamic equilibrium) and boundary conditions. Terms of equal powers are collected, providing problems that are solved in increasing order of ε-powers. That requires that the fields have been scaled beforehand according to the phenomena, see Section 3.3.

3.2 Two-scale phenomena

Collective excitation of the city structures. Set in motion by the seismic field, the buildings on the surface Γ oscillate and act as mutually interacting secondary sources. Owing to the linearity in the system, all the elements oscillate at the imposed frequency $f = \omega/2\pi$ (the time-dependence $\mathrm{e}^{-i\omega t}$ will be implicit in the sequel). In its motion, each building exerts upon its foundation S the force **F** and the moment **M** while the surface outside the foundation is free, see Fig. 3. That results in the heterogeneous distribution of stresses **t** applied at the surface

of the elastic substrate to balance the force **F** and moment **M** under the foundation, while **t** = **0** at the free surface. Without specifying any further the stress vector **t**, it is clear that it varies at the wavelength scale (forced by the seismic field) while being locally Σ-periodic at the scale of the periods (produced by the periodic array of buildings). As a result, the stress **t** depends on both space variables, that is, $\mathbf{t}(\mathbf{x}_\Gamma, \mathbf{y}_\Gamma)$, where the index $_\Gamma$ denote the projection on the surface Γ.

Localization of small-scale perturbations. The seismic field, which displays significant variations upon long-wavelength distances only, cannot balance the two-scale stresses $\mathbf{t}(\mathbf{x}_\Gamma, \mathbf{y}_\Gamma)$ on its own, because of a scale-mismatch with the local periodicity. To fulfil the scale-transition between the long-wavelength seismic field and the sub-wavelength city arrangement, a boundary layer is formed in the vicinity of the surface (Boutin & Roussillon 2006), see Sánchez-Palencia (1980) and Holloway & Kuester (2000) in other domains of physics. Superimposed upon the long-wavelength field to satisfy the locally periodic boundary conditions, and localized near the city, the Boundary Layer (BL) is made of evanescent waves which fade away at some distance from the surface.

3.3 Governing equations

Long-wavelength field. Far from the surface Γ, only the long-wavelength field prevails, with the displacement **u**(**x**) and stress tensor $\sigma(\mathbf{x})$. Its propagation is governed by the usual equations of elastodynamics expressed with the macrovariable **x**. Denoting $\mathbf{e}_x(\mathbf{u}) = [\mathbf{grad}_x(\mathbf{u}) + {}^t\mathbf{grad}_x(\mathbf{u})]/2$ the tensor of small strains (with respect to the macrovariable **x**), and reminding that $\mathbf{e}_y[\mathbf{u}(\mathbf{x})] = \mathbf{0}$ and $\mathbf{div}_y[\sigma(\mathbf{x})] = \mathbf{0}$ because the long-wavelength fields are independent from **y**, the following equations hold:

$$\sigma = \mathbf{C} : \mathbf{e}_x(\mathbf{u}); \tag{2a}$$

$$\mathbf{div}_x(\sigma) = -\rho\omega^2\mathbf{u}, \tag{2b}$$

where **C** is the elastic tensor and ρ the density of the elastic medium. At this stage, the effective boundary condition satisfied by the long-wavelength field on the surface Γ is unknown. It will be provided by the equilibrium of the boundary layer in the vicinity of the city.

Boundary Layer (BL). Near the surface Γ, the equations of elastodynamics are satisfied by the superposition of the long-wavelength field and the BL fields. Since the boundary layer fields, with the displacement $\mathbf{u}^\star$ and the stress tensor $\sigma^\star$, are locally periodic, they depend on the microvariable **y**, namely $\mathbf{u}^\star(\mathbf{x}_\Gamma, \mathbf{y})$ and $\sigma^\star(\mathbf{x}_\Gamma, \mathbf{y})$. The elastodynamic equations thus involve the **y**-differentiation and take the form:

$$\sigma + \sigma^\star = \mathbf{C} : [(\mathbf{e}_x + \varepsilon^{-1}\mathbf{e}_y)(\mathbf{u} + \mathbf{u}^\star)]; \tag{3a}$$

$$(\mathbf{div}_x + \varepsilon^{-1}\mathbf{div}_y)(\sigma + \sigma^\star) = -\rho\omega^2(\mathbf{u} + \mathbf{u}^\star). \tag{3b}$$

By subtraction with the set of equations (2) governing the long-wavelength field, the following equations are found, which govern the BL fields:

$$\sigma^\star = \mathbf{C} : [(\mathbf{e}_x + \varepsilon^{-1}\mathbf{e}_y)(\mathbf{u}^\star)]; \tag{4a}$$

$$(\mathbf{div}_x + \varepsilon^{-1}\mathbf{div}_y)(\sigma^\star) = -\rho\omega^2\mathbf{u}^\star. \tag{4b}$$

At some distance away from the city, that is, as $\mathbf{y} \cdot \mathbf{n} \to -\infty$ in the local description, the evanescence of the boundary layer is given by the conditions:

$$\mathbf{u}^\star \to \mathbf{0} \quad \text{and} \quad \sigma^\star.\mathbf{n} \to \mathbf{0} \quad \text{as} \quad \mathbf{y} \cdot \mathbf{n} \to -\infty. \tag{5}$$

Recall also that the BL fields fulfil the 2-D Σ-periodicity with respect to the microvariable **y**.

Boundary conditions. As mentioned previously, the total stress field $\sigma + \sigma^\star$ balances the surface stresses **t** at the period Σ:

$$(\sigma + \sigma^\star).\mathbf{n} = \mathbf{t} \quad \text{at } \Sigma. \tag{6}$$

That condition can be detailed as follows in the case of buildings on rigid foundations arranged on an otherwise free surface: Outside the foundations *S*, the surface $\Sigma_f = \Sigma \backslash S$ of the period Σ is free:

$$\mathbf{t} = \mathbf{0} \quad \text{at } \Sigma_f = \Sigma \backslash S. \tag{7}$$

At the foundation *S*, the force **F** and moment **M** are balanced by the surface stresses **t**. Denoting $\mathbf{y}_S$ the centre of the foundation in the local description, the following conditions hold:

$$\int_S \mathbf{t} \, dS_y = \mathbf{F}; \quad \int_S (\mathbf{y} - \mathbf{y}_S) \wedge \mathbf{t} \, dS_y = \mathbf{M}. \tag{8}$$

Finally, the foundation *S* imposes a rigid-body motion to the elastic medium, with the translation $\mathbf{u}_S$ and the rotation vector θ_S; the kinematic compatibility condition reads:

$$\mathbf{u} + \mathbf{u}^\star = \mathbf{u}_S + \theta_S \wedge (\mathbf{y} - \mathbf{y}_S) \quad \text{at } S. \tag{9}$$

Here, the local boundary conditions account explicitly for the rigid body motion of the foundation, contrary to Boutin & Roussillon (2006). Note that, in principle, the rotation vector θ_S is 3-D and thus accounts for the rocking of the foundation in both horizontal directions, and for the torsion around the normal axis. However, in practice, for sufficiently regular structures, the torsion induced by translation motions in the soil can be disregarded in comparison to rocking.

Scaling of the BL fields. Situations are considered where the buildings are strongly coupled through multiple Structure-Soil-Structure Interactions (SSSIs), which implies that the boundary layer plays an effective role in the equilibrium of the city. For this to be realized, the surface forces **t**, the long-wavelength stress σ, and the BL stress $\sigma^\star$ should be of the same order of magnitude:

$$\sigma^\star = \mathcal{O}(\sigma) = \mathcal{O}(\mathbf{t}). \tag{10}$$

However, according to the constitutive laws in eqs (2a) and (4a), the following relations also hold:

$$\sigma = \mathcal{O}(\mathbf{C}k\mathbf{u}) \quad \text{and} \quad \sigma^\star = \mathcal{O}(\mathbf{C}\mathbf{u}^\star/\ell), \tag{11}$$

and consequently, eq. (10) implies:

$$\mathbf{u}^\star = \mathcal{O}(\varepsilon\mathbf{u}). \tag{12}$$

In other words, the long-wavelength displacement $\mathbf{u}(\mathbf{x})$ prevails on the locally varying BL motions.

3.4 Homogenization results—city-impedance

Following Boutin & Roussillon (2006), the homogenization method described in Section 3.1 is conducted. It relies on the integration of the elastodynamic equations upon the volume Ω of medium located normally to the period Σ, see Fig. 3. The derivation is given in Appendix. The present paragraph provides the main results.

Long-wavelength description of the seismic field. At the leading order of the asymptotic expansions, the long-wavelength description of the seismic field relies on the two following results: (1) the long-wavelength displacement field is dominant upon the BL field; and (2) the long-wavelength stress σ is shown to balance the mean stress experienced by the period Σ, that is, the following boundary condition is derived at each period Σ of the surface Γ:

$$\sigma.\mathbf{n} = \mathbf{F}/|\Sigma|. \tag{13}$$

This effective boundary condition, found here from boundary conditions (6)–(9) at the local scale, is similar to that found by Boutin & Roussillon (2006) in the case of prescribed surface stresses. Since only the resulting force **F** is relevant to the long-wavelength field: (1) the knowledge of the exact arrangement of the resonant buildings on the period Σ is not required; and (2) the local distribution of moments **M** has no direct effect on the boundary conditions.

City-impedance. The force **F** and moment **M** depend on the rigid-body motion of the foundations through the frequency-dependent impedance matrices $\mathbf{Z}_t$, $\mathbf{Z}_r$, $\mathbf{Z}_c$ and $\mathbf{Z}'_c$ which characterize the buildings' behaviour:

$$\begin{pmatrix} \mathbf{F} \\ \mathbf{M} \end{pmatrix} = -i\omega \begin{bmatrix} \mathbf{Z}_t & \mathbf{Z}_c \\ \mathbf{Z}'_c & \mathbf{Z}_r \end{bmatrix} \cdot \begin{pmatrix} \mathbf{u}_S \\ \theta_S \end{pmatrix}. \tag{14}$$

Since the motion at the leading order consist of the long-wavelength field **u**, the dominant motion of the foundations is the uniform translation $\mathbf{u}_S = \mathbf{u}(\mathbf{x}_\Gamma)$, while the rotation of the foundation stems from the BL field $\mathbf{u}^\star = \mathcal{O}(\varepsilon\mathbf{u})$ one order smaller. Thus, the effects of the foundation rotation can be disregarded as a first approximation and the force **F** is given by: $\mathbf{F} = -i\omega\mathbf{Z}_t\mathbf{u}_\Gamma$ where $\mathbf{u}_\Gamma = \mathbf{u}(\mathbf{x}_\Gamma)$. Using eq. (13), the following boundary condition is derived for the long-wavelength field:

$$\sigma.\mathbf{n} = -i\omega\mathbf{Z}_\Gamma.\mathbf{u}_\Gamma; \quad \mathbf{Z}_\Gamma = \mathbf{Z}_t/|\Sigma| \quad \text{on } \Gamma, \tag{15}$$

where $\mathbf{Z}_\Gamma$ is the effective city-impedance at the leading order. According to the buildings properties in the different directions, anisotropic and frequency-dependent effects can arise in the supporting elastic medium despite its own isotropy and elasticity, see Section 4.1.

BL corrections. For a more comprehensive description, the BL kinematics of the foundation (the rotation θ_S and the additional translation $\mathbf{u}^\star_S = \mathbf{u}_S - \mathbf{u}_\Gamma$) induced by the field $\mathbf{u}^\star$ can be included in the previous analysis. It can be shown (see Appendix) that these BL kinematics are forced linearly by the force **F** and moment **M** applied to the foundation. That leads to the definition of the BL flexibility matrices $\mathcal{S}_t$, $\mathcal{S}_r$, $\mathcal{S}_c$ and $\mathcal{S}'_c$ through the relations:

$$\begin{pmatrix} \mathbf{u}^\star_S \\ \theta_S \end{pmatrix} = \begin{bmatrix} \mathcal{S}_t & \mathcal{S}_c \\ \mathcal{S}'_c & \mathcal{S}_r \end{bmatrix} \cdot \begin{pmatrix} \mathbf{F} \\ \mathbf{M} \end{pmatrix}. \tag{16}$$

These flexibility matrices stem from the boundary layer equilibrium and depend therefore on the city arrangement. Similar formulations can be found for local soil/foundation interaction regarding an isolated building (Wolf 1994; Sieffert & Cevaer 1992). Denoting **I** the 3 × 3 identity matrix, the combination of eqs (14) and (16) with the relation $\mathbf{u}_S = \mathbf{u}_\Gamma + \mathbf{u}^\star_S$ leads to the relations:

$$\mathbf{F} = -i\omega\mathbf{Z}_F\mathbf{u}_\Gamma; \quad \mathbf{M} = -i\omega\mathbf{Z}_M\mathbf{u}_\Gamma, \tag{17}$$

where

$$
\begin{bmatrix} \mathbf{Z}_F \\ \mathbf{Z}_M \end{bmatrix} = \left\{ \begin{bmatrix} \mathbf{I} & \mathbf{0} \\ \mathbf{0} & \mathbf{I} \end{bmatrix} + i\omega \begin{bmatrix} \mathbf{Z}_t & \mathbf{Z}_c \\ \mathbf{Z}'_c & \mathbf{Z}_r \end{bmatrix} \begin{bmatrix} \mathcal{S}_t & \mathcal{S}_c \\ \mathcal{S}'_c & \mathcal{S}_r \end{bmatrix}^{-1} \right\} \begin{bmatrix} \mathbf{Z}_t \\ \mathbf{Z}'_c \end{bmatrix}. \tag{18}
$$

Despite the 6 degrees of freedom for the foundation, eq. (17) shows that the system is driven by the long-wavelength field $\mathbf{u}_\Gamma$ only and the city-impedance can be defined as $\mathbf{Z}_\Gamma = \mathbf{Z}_F/|\Sigma|$. It includes corrections from the boundary layer and, in particular, from the rotation of the foundation induced by the moment that the slender structure applies.

Remarks. The general problem of 'wave/structure interaction' in seismic engineering is usually split into two problems: (1) the mutual interactions between structures through the soil, the so-called SSSI; and (2) the global effect of the structures on the soil motion. In the case (1), the mutual interactions do not modify the seismic excitation: It remains the one that would exist if the structures were not present at the surface, see for instance Luco & Contesse (1973) or Wong & Trifunac (1975) in 2-D. In the case (2), the global response of the vast collection of structures is seen as the superposition of the responses of each structure, but usually with the individual response that they would have if they were isolated on the half-space, for example, Guéguen *et al.* (2002).

In the present 3-D model, all the structures are in mutual interaction with one another, *and* their collective response modify the global seismic field. This is intrinsically related to the local periodicity condition that is imposed to the ground motion field (i.e. to the boundary layer). As a result, the existence of neighbouring structures and the subsequent mutual interactions are necessarily taken into account. This condition of local periodicity makes the difference with the conditions of isolated radiation in half-space made in the case (2). Further, the combination of all the interacting responses of the structures modifies the global soil motion (through the equivalent impedance condition).

4 CITY-IMPEDANCE MODEL

The previous section has derived the effective surface impedance of the periodic city arrangement from the structural properties (mechanical impedances) of the constitutive structures. In this section, those impedances are specified and the effects of the city-impedance are investigated. In particular, the problem of interaction between the city and a soil layer is addressed.

4.1 Unconventional effects of the city-impedance

Equivalent SDOF oscillator. Using modal analysis, the fundamental mode of the structure can be characterized by a Single-Degree-Of-Freedom (SDOF) oscillator with the mass m_o, stiffness K and damping c in one horizontal direction. Focusing on this direction, the problem is scalar. The motion u_Γ at the surface induces the motion u_o of the mass m_o while the force F that the oscillator exerts on the period Σ balances the oscillator's inertia. Newton's Second Law provides

$$
F = m_o \omega^2 u_o = (K - i\omega c)(u_o - u_\Gamma). \tag{19}
$$

Defining the eigenfrequency $f_o = \omega_o/2\pi = (2\pi)^{-1}\sqrt{K/m_o}$ and the damping ratio $\xi = c/2\sqrt{Km_o} \ll 1$, the transfer function u_o/u_Γ and the impedance $Z = F/(-i\omega u_\Gamma)$ of the oscillator take the form:

$$
\frac{u_o}{u_\Gamma} = \frac{1 - i2\xi\frac{\omega}{\omega_o}}{1 - i2\xi\frac{\omega}{\omega_o} - \frac{\omega^2}{\omega_o^2}}; \quad Z = i\omega m_o \frac{u_o}{u_\Gamma}. \tag{20}
$$

This provides the city impedance $Z_\Gamma = Z/|\Sigma|$ in the horizontal direction of resonance. Normalized by the shear impedance of elastic substrate $Z_s = \rho c_s = \sqrt{\rho\mu}$, it reads:

$$
\frac{Z_\Gamma}{Z_s} = \eta \frac{i\frac{\omega}{\omega_o}\left(1 - i2\xi\frac{\omega}{\omega_o}\right)}{1 - i2\xi\frac{\omega}{\omega_o} - \frac{\omega^2}{\omega_o^2}}; \quad \eta = \frac{\sqrt{Km_o}}{|\Sigma|\sqrt{\mu\rho}} = \frac{m_o\omega_o}{|\Sigma|\sqrt{\mu\rho}}. \tag{21}
$$

Frequency-dependent switch from free to 'rigid' boundary. According to eq. (21), the free surface condition ($Z_\Gamma = 0$) is recovered with $\eta = 0$ while heavy and rigid buildings (compared to the soil) produce substantial interactions, see the expression of η. The normalized impedance Z_Γ/Z_s is shown against frequency in Fig. 4 with the value $\eta = 0.1$. At low and high frequency ($\omega \ll \omega_o$ or $\omega \gg \omega_o$ respectively), the city-impedance Z_Γ is much smaller than the soil impedance Z_s similarly to the usual free surface condition. Conversely, around resonance $\omega \approx \omega_o$ of weakly damped oscillators $\xi \ll 1$, the impedance ratio reaches the negative value $Z_\Gamma/Z_s = -\eta/2\xi$ which is large provided that $\eta/2\xi \gg 1$, similarly to a rigid condition imposed in the oscillator's direction only.

Frequency-dependent anisotropy. The SDOF model can be applied in both horizontal principal directions of the building/BL system around its first modes, say in directions X and Y. To discriminate the effects of resonance, the system is supposed to experience a resonance in the X-direction but no resonance (i.e. the structure remains inert) in the Y-direction within the frequency range of the scale separation. For more accuracy in the description, the total mass of the structure is accounted for: If m_o is the modal mass of the structure in the X direction, m_i is the complementary mass of the structure not involved in that mode (its motion is the displacement u_Γ). In the inert Y direction, the total
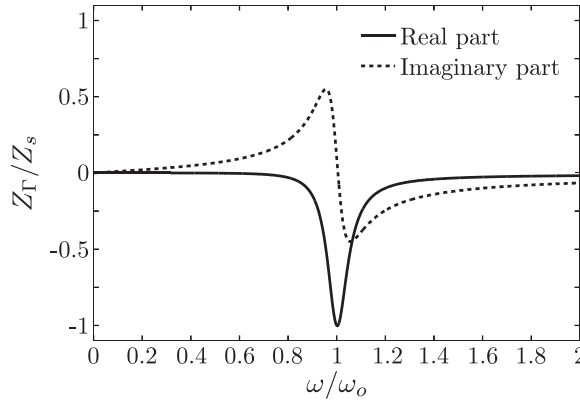
Figure 4. Real and imaginary parts of city-impedance Z_Γ against frequency ω. City-impedance normalized by soil shear impedance Z_s; frequency normalized by the eigenfrequency ω_o of the city. Calculations performed with $\eta = 0.1$ and $\xi = 5$ per cent.

mass $m = m_o + m_i$ of the structure is an inert mass. Focusing on the two principal directions, the problem is planar and the city impedance matrix takes the form $\mathbf{Z}_\Gamma = Z_X \mathbf{e}_X \otimes \mathbf{e}_X + Z_Y \mathbf{e}_Y \otimes \mathbf{e}_Y$ where:

$$\frac{Z_X}{Z_s} = i\eta \left(\frac{u_o}{u_\Gamma} + \frac{m_i}{m_o} \right) \frac{\omega}{\omega_o}; \qquad \frac{Z_Y}{Z_s} = i\eta \left(1 + \frac{m_i}{m_o} \right) \frac{\omega}{\omega_o} \,. \tag{22}$$

The anisotropy $Z_X \neq Z_Y$ leads to depolarization phenomena (Boutin *et al.* 2015) and atypical mode conversions (Schwan & Boutin 2013).

Remark. In the case where the city-impedance includes the BL corrections, it can be shown that the SDOF model in eqs (20) and (21) still holds around resonance provided that ω_o and ξ are apparent modal parameters accounting for the local soil/foundation interaction, see Schwan (2014).

4.2 Site-city interaction

In the aim of experimental and numerical validations, the city effects expected from the theory are presented when the city, characterized by eq. (22), is settled at the surface of an elastic layer (thickness $H \gg \ell$) resting on a rigid substratum.

Site-city interaction model. The site-city interaction is derived from the response of the site-city system to a harmonic horizontal displacement $\mathbf{u}_b$ imposed at the base of the layer. Solving the wave equation, the horizontal displacement takes the form $\mathbf{u}(z) = \mathbf{U}_c \cos(\omega z/c_s^*) + \mathbf{U}_s \sin(\omega z/c_s^*)$ where z is the upward vertical abscissa, $c_s^* = c_s \sqrt{1 - i2\xi_s}$ is the complex shear-wave speed and $\mathbf{U}_c$ and $\mathbf{U}_s$ are complex amplitudes given by the boundary conditions. The displacement $\mathbf{u}(z)$ satisfies the city-impedance condition (15) at the surface $z = 0$ and is equal to the displacement $\mathbf{u}_b$ at the surface $z = -H$ of the layer. Introduce $f_H = \omega_H/2\pi = c_s/4H$ the eigenfrequency of the layer with a free surface, and the complex quantities $Z_s^* = \rho c_s^*$ and $\omega_H^*/2\pi = c_s^*/4H$. Solving for the amplitudes $\mathbf{U}_c$ and $\mathbf{U}_s$ in the principal axes X and Y of the impedance matrix $\mathbf{Z}_\Gamma$ provides the surface displacement $\mathbf{u}_\Gamma = \mathbf{u}(z = 0)$:

$$\mathbf{u}_\Gamma \cdot \mathbf{e}_X = \left[\cos \left(\frac{\pi}{2} \frac{\omega}{\omega_H^*} \right) + i \frac{Z_X}{Z_s^*} \sin \left(\frac{\pi}{2} \frac{\omega}{\omega_H^*} \right) \right]^{-1} \mathbf{u}_b \cdot \mathbf{e}_X;$$

$$\mathbf{u}_\Gamma \cdot \mathbf{e}_Y = \left[\cos \left(\frac{\pi}{2} \frac{\omega}{\omega_H^*} \right) + i \frac{Z_Y}{Z_s^*} \sin \left(\frac{\pi}{2} \frac{\omega}{\omega_H^*} \right) \right]^{-1} \mathbf{u}_b \cdot \mathbf{e}_Y; \tag{23}$$

and the horizontal displacement $\mathbf{u}(z)$ in the layer:

$$\mathbf{u}(z) \cdot \mathbf{e}_X = \left[\cos \left(\frac{\pi}{2} \frac{\omega}{\omega_H^*} \frac{|z|}{H} \right) + i \frac{Z_X}{Z_s^*} \sin \left(\frac{\pi}{2} \frac{\omega}{\omega_H^*} \frac{|z|}{H} \right) \right] \mathbf{u}_\Gamma \cdot \mathbf{e}_X;$$

$$\mathbf{u}(z) \cdot \mathbf{e}_Y = \left[\cos \left(\frac{\pi}{2} \frac{\omega}{\omega_H^*} \frac{|z|}{H} \right) + i \frac{Z_Y}{Z_s^*} \sin \left(\frac{\pi}{2} \frac{\omega}{\omega_H^*} \frac{|z|}{H} \right) \right] \mathbf{u}_\Gamma \cdot \mathbf{e}_Y. \tag{24}$$

Eqs (23) and (24) show that (1) at the resonance in X, the impedance ratio $|Z_X/Z_s^*| \gg 1$ makes the surface motion vanish $\mathbf{u}_\Gamma \cdot \mathbf{e}_X \to 0$ in that direction only, similarly to a rigid surface condition along $\mathbf{e}_X$; (2) since $Z_Y \neq Z_X$, the direction of the surface motion $\mathbf{u}_\Gamma$ can depart from the base motion $\mathbf{u}_b$, namely the surface motion is depolarized; and (3) the motion $\mathbf{u}(z)$ in the layer is depolarized too.

Site-city effects in the resonant direction. In the X direction, the effect of the free/rigid switch in the boundary condition is magnified when the eigenfrequency ω_o of the city belongs to the frequency range of the layer resonance, that is, close to ω_H. As shown in Fig. 5 the following phenomena are expected: (1) at the frequency at which the layer resonance should occur, a surface antiresonance happens due to the rigid-like condition imposed by city resonance; (2) the layer resonance peak is split into two soil-city resonance peaks; (3) the amplitude of those peaks is substantially reduced compared to the layer resonance peak; and (4) the phase is strongly modified. In the time domain, such a two-peak-spectrum is favourable to beatings.
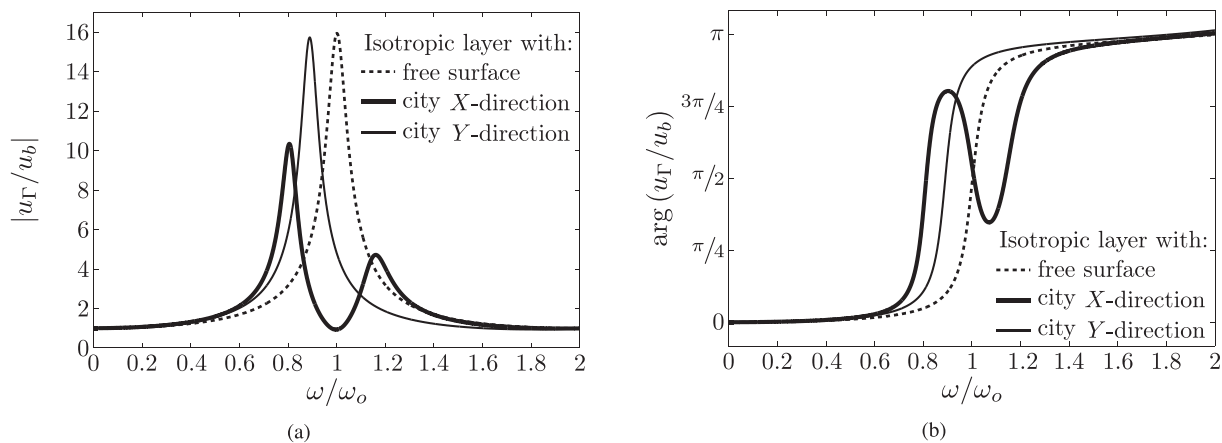
Figure 5. Transfer function between the displacement u_Γ at the top surface of the elastic layer and the input motion u_b at the base of the layer in both principal directions X (resonant) and Y (non-resonant) of the anisotropic city: (a) amplitude of u_Γ/u_b and (b) phase of u_Γ/u_b. Frequency normalized by the eigenfrequency ω_o of the city. Comparison with the case of a layer with a free surface, that is, without the city. Calculations performed with $\xi_s = 4$ per cent, $\eta = 0.1$, $m_i = m_o$, $\omega_H = \omega_o$ and $\xi = 5$ per cent.

Site-city effects in the non-resonant direction. In the Y direction, the city is non-resonant and the impedance ratio Z_Y/Z_s^* is given in eq. (22). When $\eta(1 + m_i/m_o)$ is small compared to 1, the transfer functions in eqs (23) and (24) tend to those of a layer with a free surface:

$$\mathbf{u}(z) \cdot \mathbf{e}_Y \approx \left[\cos\left(\frac{\pi}{2} \frac{\omega}{\omega_Y^*} \frac{|z|}{H} \right) \right] \left[\cos\left(\frac{\pi}{2} \frac{\omega}{\omega_Y^*} \right) \right]^{-1} \mathbf{u}_\Gamma \cdot \mathbf{e}_Y \tag{25}$$

with the apparent resonance frequency $\omega_Y^* \approx \omega_H^*(1 + \frac{m}{\rho|\Sigma|H})^{-1}$. That latter is lower than the layer eigenfrequency ω_H^* because of the additional mass $m = m_o + m_i$ provided by the city at the top surface. This phenomenon is shown in Fig. 5. Note that the inert mass m_i in the X-direction has also the effect to reduce the layer eigenfrequency to the value $\omega_X^* \approx \omega_H^*(1 + \frac{m_i}{\rho|\Sigma|H})^{-1}$.

Discussion. Despite different physical origins, the observations made in the resonant X-direction (double-peak resonance, antiresonance trough, modified phase) recall those described in dynamics when two co-resonant mass-spring systems are associated (Hartog 1956). Numerical simulations, reported by Wirgin & Bard (1996), Clouteau & Aubry (2001), Semblat *et al.* (2008) and Groby & Wirgin (2008) have shown similar splits of the layer resonance when adding resonant structures at the top surface of an elastic layer. However, comparisons are not straightforward due to different sets of configurations, hypotheses and frequency ranges in the models. That is why: (1) the CIM will be compared with a BEM based on similar assumptions; and (2) both models will be validated against shaking table measurements on a specifically devised site-city experimental setup.

5 EXPERIMENTAL SETUP

In this section, the experimental setup is designed on the basis of the city-impedance analysis in order to evidence the site-city effects predicted theoretically in Section 4.

5.1 Description and design

Description of the setup. The idealized small-scale city consists of 37 identical resonating structures arranged periodically with a centre-to-centre spacing $\ell = 5$ cm, see Fig. 6(a). They are glued at the top surface an elastic layer with cellular polyurethane foam as soil analogue material (density $\rho = 49$ kg m^{-3}, shear modulus $\mu = 55$ kPa, Poisson ratio $\nu = 6$ per cent, damping $\xi_s = 4.9$ per cent, giving $c_s = 33$ m s^{-1}) so as to respect the theoretical assumptions (homogeneity, linearity) in a large range of deformation. Each resonant structure is made up of a vertical aluminium sheet (density $\rho_{Al} = 2700$ kg m^{-3}, Young modulus $E_{Al} = 69 \times 10^9$ Pa, Poisson ratio $\nu_{Al} \approx 0.3$) sandwiched along its lowermost edge between two rigid aluminium angles to provide a footing with the width $2b = 2 \times 1.3$ cm, see Figs 6(b) and (c). The sheet has the length $\mathcal{L} = 1.75$ m, thickness $e = 0.5$ mm and height h out of the angles, Fig. 6(c). It can resonate in bending in response to an out-of-plane motion of the footing (direction $\mathbf{e}_X$); it remains quasi-inert when excited with an in-plane motion (horizontal direction $\mathbf{e}_Y \perp \mathbf{e}_X$). The system is secured to the platform of the shaking table through a base-plate assembly.

Equivalent SDOF oscillators for the resonators. Since the modal frequencies of a clamped-free bending beam are well separated (according to the series $\omega_j/\omega_o \approx \{1 ; (3/1.2)^2 ; (5/1.2)^2 ; \dots\}$), the bending sheet can be modelled, in the X-direction and in the frequency range close to the first mode (say $\omega \lesssim 2\omega_o$), as a SDOF oscillator associated with an inert mass m_i. The SDOF oscillator is characterized by: the modal mass $m_o \approx 0.613 \rho_{Al} \mathcal{L} e h$ of the sheet; the eigenfrequency $\omega_o/2\pi$ of the bending structure; and the weak damping $\xi \ll 1$. The top motion u_{sheet} of the sheet in the X-direction is related around resonance to the motion u_o of the equivalent SDOF oscillator by
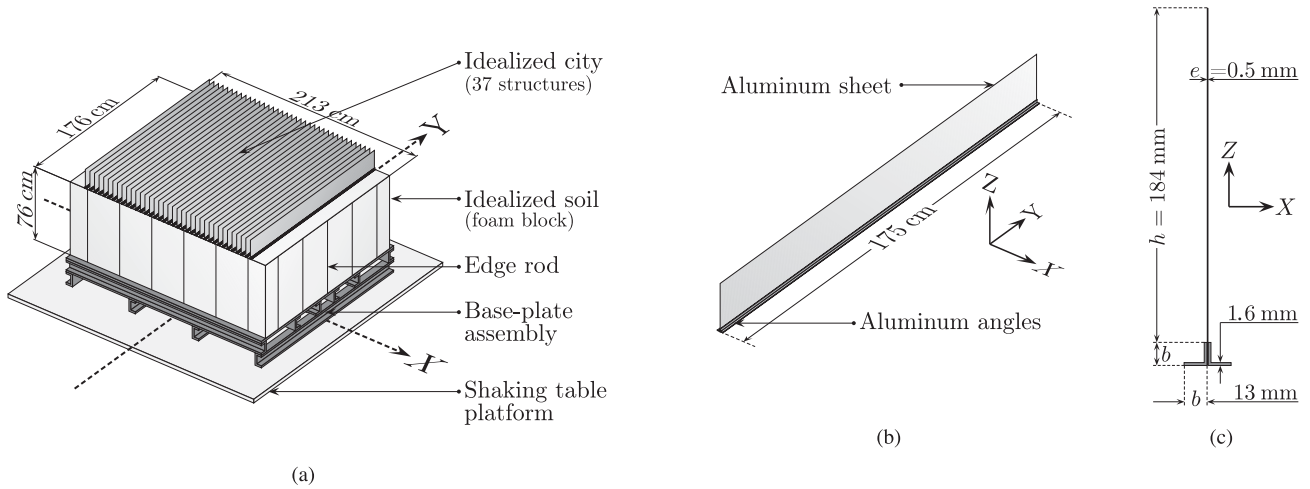
Figure 6. Schematic of the experimental site-city setup. (a) Overall view of the experimental setup on the shaking table: 37 resonators are arranged periodically at the top surface of an elastic layer. (b) Detail of one anisotropic resonator: an aluminium sheet is sandwiched at its lowermost edge between a pair of angles; it can resonate in bending in the out-of-plane X direction but not in the in-plane direction Y. (c) Dimensions of the resonant structure in a cross-section.

$u_{sheet} = \chi u_o$ where the geometrical coefficient $\chi \approx 1.57$ is derived theoretically from the first mode shape of a bending beam (Schwan 2014). In the direction Y, all the mass $m = m_o + m_i$ is inert.

Design. The system is designed so that: The scale separation is satisfied at city eigenfrequency ($\varepsilon_o = \ell\omega_o/c_s \ll 1$); the city-impedance is significant compared to the soil one ($\eta/2\xi \geq \mathcal{O}(1)$); and the shear resonance frequency ω_H of the layer (with a free surface) is close to the city eigenfrequency ω_o in order to magnify site-city interactions. For that purpose, the sheets are $h = 18.4$ cm-high outside the angles, which provides (theoretically) the modal mass $m_o = 0.266$ kg, and the total mass $m_o + m_i = 0.849$ kg and (experimentally) the city eigenfrequency $\omega_o/2\pi = 8.45$ Hz and the damping $\xi \approx 4$ per cent. That leads to the small scale parameter $\varepsilon_o = 0.08$ at city eigenfrequency while the parameter $\eta = 11.5$ per cent makes $\eta/2\xi \approx 1.44$. The foam block is 2.13 m wide in X and 1.76 m wide in Y and has the thickness $H = 0.76$ m. That provides the shear resonance frequencies 9.36 Hz and 9.11 Hz for the foam block in the directions X and Y respectively. The repeatability and linearity of the system have been checked experimentally in the frequency range [0; 20] Hz.

Remarks. To prevent the gyration mode of the foam block, that is, its rotation around the horizontal axis similarly to a bending motion, that could develop in addition to the shear translation motion, 22 thin vertical steel rods (3 mm diameter and 75 cm long) are adhered at 35 cm centres around the periphery of the foam block, see Fig. 5(a). Their diameter and spacing are designed not to disturb the shear block's modes (i.e. their bending stiffness is much smaller than the shear stiffness of the foam block) while restraining parasite vertical edge movements (i.e. their elongation stiffness is much larger than that of the foam block).

5.2 Other configurations

To analyse the influence of city-density on site-city interactions, four other configurations have been tested in addition to the full city-arrangement described here-above: Three periodic city-arrangements with the period sizes 2ℓ (19 resonators), 4ℓ (9 resonators) and 8ℓ (5 resonators), and one isolated structure on the foam block, see Fig. 7. Those configurations challenge the CIM and its scale-separation assumption: The wider periods Σ weaken the scale parameter according to $2\varepsilon_o = 0.16$, $4\varepsilon_o = 0.32$ and $8\varepsilon_o = 0.64$ respectively. The CIM will be considered despite the poor scale separations, in order to assess the robustness of the model.

5.3 Instrumentation and excitations

Instrumentation. Measurements are performed with 3-D-accelerometers located on the foam block (on the top and lateral surfaces, Fig. 8) and at the top of four resonant structures, Fig. 7. The reference input motion is recorded by accelerometers on the shaking table. Two types of accelerometers are used: Where mass of the sensor could have a deleterious effect on the response (at the top of some sheets) and where little space is available (on the foam block between two structures), low-mass MEMS accelerometers are used (Analog Devices ADXL335, 2 gram mass, 2 cm wide footprint); otherwise, Setra type 141A accelerometers are used. The position of the accelerometers on the elastic block enables to study the spacial variability of the top surface motion and the shear-deformation shapes in the principal directions X and Y.

Excitations. Excitation is provided by the motion of the shaking table in either the resonant X-direction, or the non-resonant Y-direction, or the horizontal direction making an angle of $45°$ with X (so as to evidence depolarization effects). The level of the excitation is a compromise between small deformations requirement and good accuracy of the measurements. Input signals consist of Ricker wavelets and sinusoidal waveforms. The Ricker wavelets have the displacement $u_{Ricker} \propto (2a(t) - 1)e^{-a^2(t)}$ with $a(t) = \pi f_r(t - t_r)$ where f_r is the central frequency and t_r the time delay. In the frequency domain, Ricker wavelets (with spectral acceleration peak around 8 Hz) provide the transfer functions with a low level of noise without windowing nor averaging (transfer functions have been confirmed by white noise); in the time domain
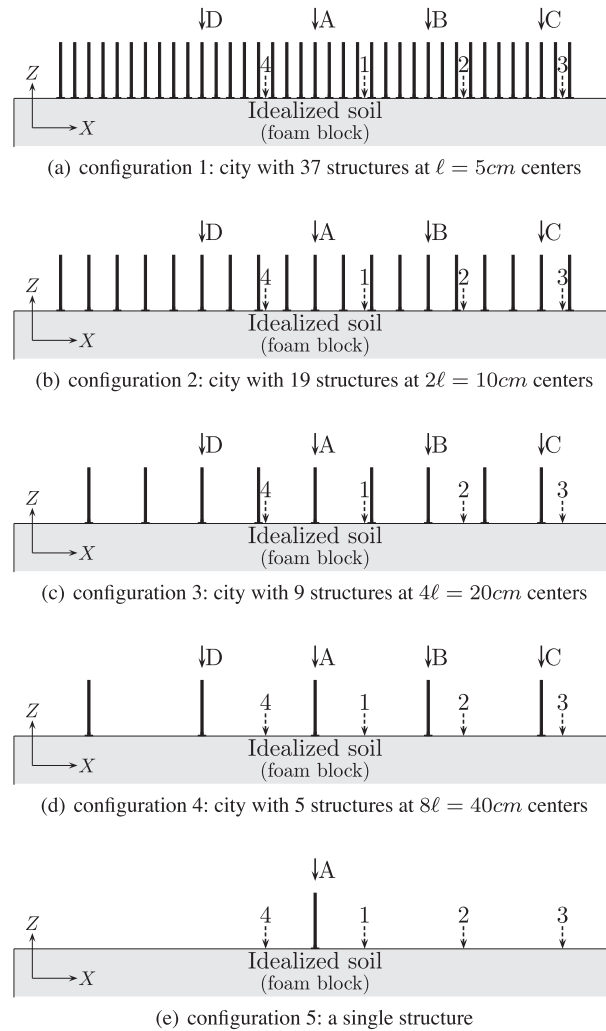
Figure 7. Schematic at scale of the different configurations for the site-city setup: Position of the resonant structures on the elastic block in the cross-section plane (X, Z). The arrows with plain line indicate the structures (A, B, C and D) instrumented with a MEMS accelerometer at their top. The arrows with dashed line (named 1 to 4) indicate the position of MEMS accelerometers on the 'free' surface of the elastic block between resonators.
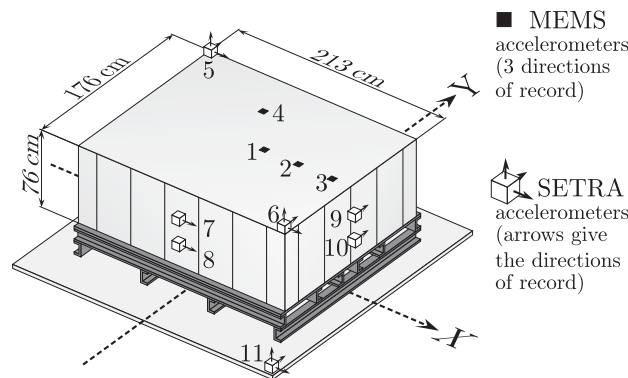

Figure 8. Instrumentation of the elastic block. Two types of accelerometers are used: low-mass MEMS and Setra accelerometers.

they give the decay response of the system. Sinusoidal waveforms are used to evidence accurately mode shapes modifications and wavefield depolarization at the (anti-) resonance frequencies of the city/layer coupled system.

6 BOUNDARY ELEMENTS MODEL

Independently from the CIM, site-city interactions can be simulated at geophysical scales by means of numerical methods applied to the elastodynamic equations, see the Introduction. For 2-D configurations and in-plane wavefield, a harmonic numerical model based on boundary
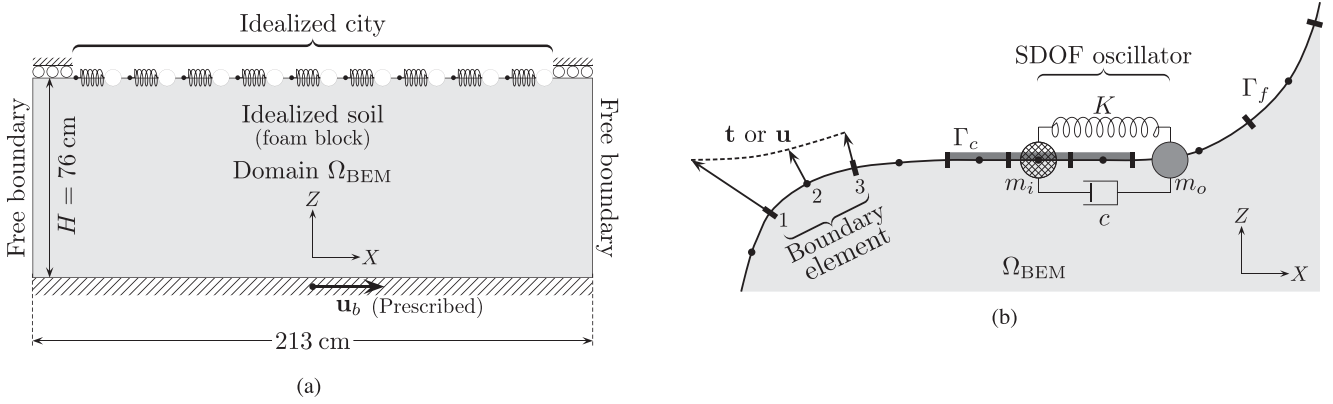
Figure 9. Boundary Elements Model (BEM) for the resonant structures on an elastic medium: (a) BEM for the soil layer; (b) SDOF oscillator for the resonant structures of the city and details of the coupling with BEM soil layer. The arrangement and size of the oscillators in panel (a) and deformation of the surface in panel (b) are purely illustrative.

elements (Padrón *et al.* 2004) is applied to the small-scale experimental setup as an independent study-case. This section presents briefly the modelling assumptions made in the numerical model; their similarities and differences with those from the CIM; and the numerical procedure.

6.1 Boundary elements soil-city model

The direct BEM is used to analyse the elastic substrate (domain Ω_{BEM}), while the resonant structures are modelled as linear-elastic 1-D horizontal oscillators.

BEM layer. The material domain Ω_{BEM} has the same dimensions as the foam block in the experimental setup (Fig. 9a). Like the layer in the CIM, it has the same physical properties as those found experimentally (density $\rho = 49\,\mathrm{kg\,m^{-3}}$, damping $\xi_s = 4.9$ per cent and Poisson's ratio $\nu = 6$ per cent) while the shear modulus $\mu = 46.5\,\mathrm{kPa}$ is such that the elastic substrate (with the boundary conditions detailed hereafter) has the same shear eigenfrequency 9.36 Hz as the experimental foam block (with the edge rods). The following boundary conditions are applied to the domain Ω_{BEM}: The horizontal harmonic displacement u_b is imposed at the lowermost edge while the top surface Γ (ignoring the resonant structures) and the lateral surfaces are free. To take into account the effects of the edge rods that prevent the gyration of the top surface in the experiments, any vertical displacements are prevented near the edges $X = \pm 1.065\,\mathrm{m}$ on the top surface, see Fig. 9(a). As a result, the field here-after computed takes into account phenomena that have been left aside by the CIM (the correctors in the asymptotic expansions) and the finite lateral extension of both the elastic medium and the city (not accounted for in the site-city interaction model described in Section 4.2). The application of the BEM to the plane viscoelastic problem in the frequency domain leads to an algebraic system of equations in the following form, see for example, Domínguez (1993):

$$\mathbf{Hu} = \mathbf{Gt} \tag{26}$$

where **u** and **t** stand for the vectors of nodal displacements and tractions, respectively, and **H** and **G** are the matrices of influence. The coefficients of these latter are obtained by integration of the corresponding products of shape functions by the fundamental solution in tractions and displacements, respectively. In this study, three-nodded quadratic elements have been used in the discretization of the boundaries.

City model. To ease comparison with the CIM, each resonant structure in the numerical model is reduced to the same horizontal SDOF oscillator as those used in the CIM, see Fig. 9(b). The modal mass m_o of the structure is localized at the 'free' node of the element while the inert mass m_i is localized at the node where the oscillator is clamped to the elastic substrate. The steady-state harmonic response of the resonant structures can be described by the classic formulation:

$$(\bar{\mathbf{K}} - i\omega\mathbf{C} - \omega^2\mathbf{M})\mathbf{U}(\omega) = \mathbf{K}(\omega)\mathbf{U}(\omega) = \mathbf{F}(\omega) \tag{27}$$

where $\bar{\mathbf{K}}$, **C** and **M** are the global stiffness, damping and mass matrices respectively and **F** is the external load vector. As would be done for in-situ measurements, the resonant structures are characterized by the apparent resonance frequency and the damping ratio measured from the experimental transfer function $u_{\mathrm{sheet}}/u_\Gamma$ of the resonator. As a result, in both the CIM and the numerical model, the stiffness K of the representative SDOF oscillator is chosen so that the eigenfrequency $\omega_o = \sqrt{K_o/m_o}$ coincides with the experimental one (for each city-configuration) and the coefficient c is such that the damping ratio is the same as the experimental one, that is, $\xi = c/2\sqrt{Km_o} = 4$ per cent.

6.2 Numerical procedure

Soil-city coupling. The coupling between the domains Ω_{BEM} and the SDOF oscillators is made through plane rigid surfaces Γ_c, perfectly bonded to the surface Γ, and which stand for the rigid foundations of the resonant structures, see Fig. 9(b). Kinematic compatibility conditions and equilibrium are established between the boundary elements of a surface Γ_c and the rigid foundation of the structure attached to it. The

kinematic compatibility among the boundary element nodes of one rigid coupling surface (3 quadratic elements per rigid footing Γ_c) and the clamped node of one resonant-structure can be described by the $2N \times 3$ compatibility matrix $\mathbf{D}^i$ as:

$$\mathbf{u}^{c_i} = \mathbf{D}^i \mathbf{u}^{b_i}, \tag{28}$$

where c_i refers to the set of boundary nodes on the ith rigid coupling surface and b_i to the node at the base of the structure coupled to it, and where $\mathbf{u}^{c_i}$ and $\mathbf{u}^{b_i}$ are vectors of $2N$ and 3 components respectively, N being the number of boundary nodes in the rigid coupling surface. On the other hand, equilibrium between the resonant-structure and its foundation can be expressed through a $3 \times 2N$ equilibrium matrix $\mathbf{C}^i$ as:

$$\mathbf{f}^{b_i} = \mathbf{C}^i \mathbf{t}^{c_i}, \tag{29}$$

where $\mathbf{f}^{b_i}$ and $\mathbf{t}^{c_i}$ are vectors of 3 and $2N$ components respectively, $\mathbf{f}^{b_i}$ being the forces acting at the base of the ith structure.

Resolution. Using eqs (28) and (29) to couple the boundary elements and the SDOF oscillators systems, and after application of boundary conditions and reordering, the equations describing the dynamic response of the system can be written as in eq. (30), where n is the number of resonant-structures; indexes s and g refer, respectively, to structure and boundary-element nodes not allocated on coupling rigid boundaries; $\mathbf{H_g} \mathbf{D}^j = \mathbf{H}_{gc_j} \mathbf{D}^j$ and $\mathbf{HD}^{ij} = \mathbf{H}_{c_i c_j} \mathbf{D}^j$. The quantities $\mathbf{A}$, $\mathbf{B}$ and $\mathbf{x}$ arise from the application of boundary conditions on the boundary element equations and reordering, where $\mathbf{x}^{\mathrm{f}}$ is the vector of unknowns in the boundary element nodes on Γ_{f}, that is, not allocated on coupling rigid boundaries. The resolution of this linear algebraic system of equations for each excitation frequency yields the nodal solution at all points of interest. See Padrón *et al.* (2004) for more details about the coupling.

$$
\begin{bmatrix}
\mathbf{K}_{ss}^1 & \cdots & \mathbf{0} & \mathbf{K}_{sb}^1 & \cdots & \mathbf{0} & \mathbf{0} & \mathbf{0} & \cdots & \mathbf{0} \\
\vdots & \ddots & \vdots & \vdots & \ddots & \vdots & \vdots & \vdots & \ddots & \vdots \\
\mathbf{0} & \cdots & \mathbf{K}_{ss}^n & \mathbf{0} & \cdots & \mathbf{K}_{sb}^n & \mathbf{0} & \mathbf{0} & \cdots & \mathbf{0} \\
\mathbf{K}_{bs}^1 & \cdots & \mathbf{0} & \mathbf{K}_{bb}^1 & \cdots & \mathbf{0} & \mathbf{0} & \mathbf{C}^1 & \cdots & \mathbf{0} \\
\vdots & \ddots & \vdots & \vdots & \ddots & \vdots & \vdots & \vdots & \ddots & \vdots \\
\mathbf{0} & \cdots & \mathbf{K}_{bs}^n & \mathbf{0} & \cdots & \mathbf{K}_{bb}^n & \mathbf{0} & \mathbf{0} & \cdots & \mathbf{C}^n \\
\mathbf{0} & \cdots & \mathbf{0} & \mathbf{H_g}\mathbf{D}^1 & \cdots & \mathbf{H_g}\mathbf{D}^n & \mathbf{A}_{gg} & -\mathbf{G}_{gc_1} & \cdots & -\mathbf{G}_{gc_n} \\
\mathbf{0} & \cdots & \mathbf{0} & \mathbf{HD}^{11} & \cdots & \mathbf{HD}^{1n} & \mathbf{A}_{c_1 g} & -\mathbf{G}_{c_1 c_1} & \cdots & -\mathbf{G}_{c_1 c_n} \\
\vdots & \ddots & \vdots & \vdots & \ddots & \vdots & \vdots & \vdots & \ddots & \vdots \\
\mathbf{0} & \cdots & \mathbf{0} & \mathbf{HD}^{n1} & \cdots & \mathbf{HD}^{nn} & \mathbf{A}_{c_n g} & -\mathbf{G}_{c_n c_1} & \cdots & -\mathbf{G}_{c_n c_n}
\end{bmatrix}
\begin{bmatrix}
\mathbf{u}^{s_1} \\ \vdots \\ \mathbf{u}^{s_n} \\ \mathbf{u}^{b_1} \\ \vdots \\ \mathbf{u}^{b_n} \\ \mathbf{x}^{\mathrm{f}} \\ \mathbf{t}^{c_1} \\ \vdots \\ \mathbf{t}^{c_n}
\end{bmatrix}
=
\begin{bmatrix}
\mathbf{0} \\ \vdots \\ \mathbf{0} \\ \mathbf{0} \\ \vdots \\ \mathbf{0} \\ \mathbf{B}_{gg} \\ \mathbf{B}^{c_1 g} \\ \vdots \\ \mathbf{B}^{c_n g}
\end{bmatrix}
\tag{30}
$$

7 RESULTS AND DISCUSSION

In this section, experimental results are presented and compared to both the CIM and the BEM. The discussion focuses in particular on the phenomena predicted theoretically by the CIM.

7.1 Kinematic homogeneity

According to the CIM, the long-wavelength displacement field prevails in the elastic medium, thus ensuring a kinematic homogeneity in the layer and a group-effect in the response of the city. The kinematic homogeneity in the city configurations 1, 4 and 5 is evidenced in Fig. 10 for the layer top surface and in Fig. 11 for the resonators. Fig. 10 shows, both in the time and frequency domain, the accelerations recorded in the direction X by four accelerometers located at the top surface of the foam block, in response to a Ricker wavelet prescribed in the direction X. Fig. 11 shows the same for the accelerometers located at the top of the instrumented resonators.

As expected, records realized at the top-surface of the foam block are nearly similar and synchronized, whether there are 37 resonators (Fig. 10a), or 5 resonators (Fig. 10c), or a single resonator on the surface (Fig. 10e). Similar comments can be made about the records realized at the top of the resonators, see Figs 11(a), (c) and (e). In particular, note that all the instrumented resonators oscillate in phase with one another. These results bear testament to the quasi-homogeneous horizontal translation of the top-surface and to the subsequent in-phase response of the resonators. These properties have been observed experimentally for the other city-configurations 2 and 3 (see Fig. 7), for other excitations (white noise, sinusoidal waveform) applied either in the direction X or Y. The numerical model provides similar results too (checked on every structure).

The similarity in the different records realized at the top-surface of the foam block for a given city-configuration leads to similar transfer functions between the acceleration measured at different points of the surface and that on the shaking table, see Figs 10(b), (d) and (f). The only noticeable difference between these transfer functions for a given city-configuration is the amplification of the acceleration at the surface as the accelerometer is closer to the edge of the foam block. This parasite edge effect, which is apparent for a single resonator in
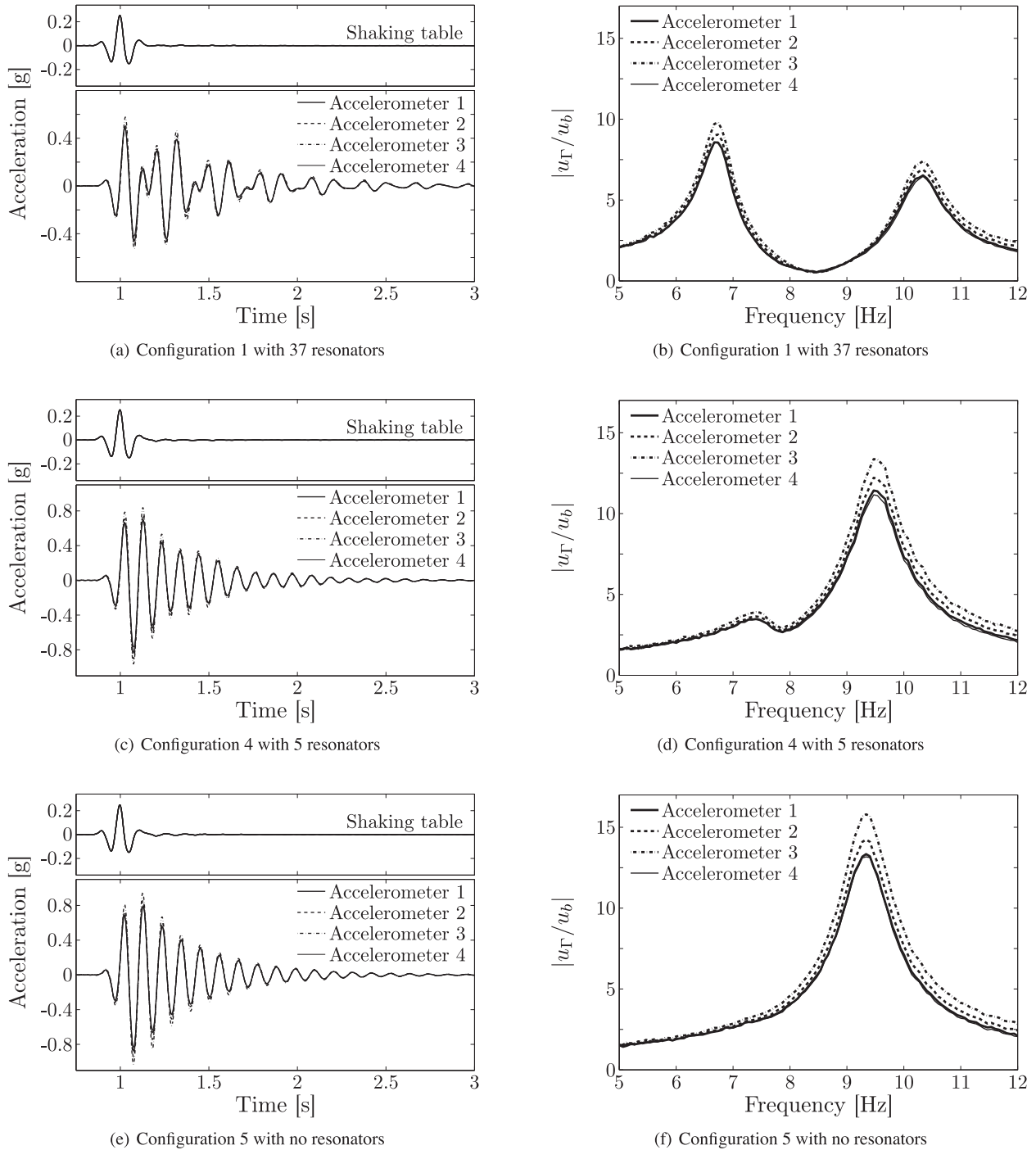
(a) Configuration 1 with 37 resonators

(b) Configuration 1 with 37 resonators

(c) Configuration 4 with 5 resonators

(d) Configuration 4 with 5 resonators

(e) Configuration 5 with no resonators

(f) Configuration 5 with no resonators

Figure 10. Kinematic homogeneity at the surface of the layer. (a, c, e) Accelerations recorded on the layer top surface by accelerometers 1 to 4 and at the shaking table in the direction X for the city-configuration 1, 4 and 5 in response to a Ricker wavelet prescribed to the shaking table in the direction X. Low-pass filter $[0, 30]$ Hz applied to the records. (b, d, f) Modulus of the transfer function in the direction X between the layer top surface motion (recorded by the accelerometers 1 to 4) and that of the shaking table for the city-configuration 1, 4 and 5.

Fig. 10(f), is also present without resonators (not presented here). It affects in similar proportions the transfer functions in the presence of the city-arrangements. Note that signals and spectra of accelerometers 1 and 4 are almost identical, which can be attributed to symmetry in the X direction. The transfer functions between the top of different resonators and the shaking table are also nearly identical for a given city-configuration. The small discrepancies can be attributed to: The parasite edge-effect of the foam block, which excites slightly differently the resonators closer to the edge than those at the centre of the foam surface; and the difference in the resonators themselves, inherent to the experimental realization.

Those observations are coherent with the macroscopic motion in the layer and the collective behaviour of the resonators that the theoretical model predicted at the leading order under the condition of scale separation. That situation is actually different from that observed
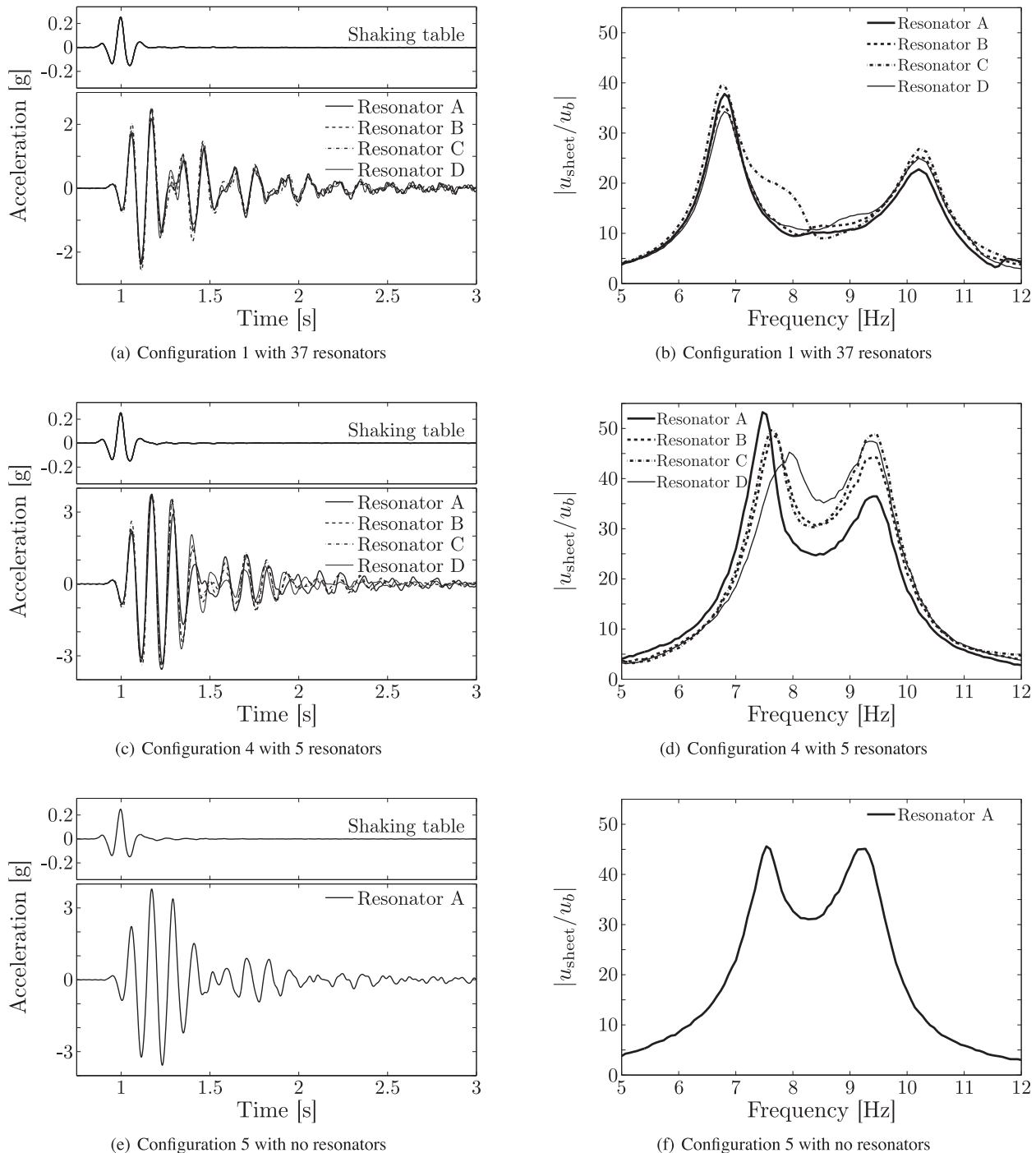
Figure 11. Kinematic homogeneity of resonators' response. (a, c, e) Accelerations recorded at the top of resonators A to D and at the shaking table in the direction *X* for the city-configuration 1, 4 and 5 in response to a Ricker wavelet prescribed to the shaking table in the direction *X*. Low-pass filter [0, 30] Hz applied to the records. (b, d, f) Modulus of the transfer function in the direction *X* between the resonators top motion (resonators A to D) and that of the shaking table for the city-configuration 1, 4 and 5.

at higher frequencies, where the signature of site-city interactions is the desynchronized motion of the structures, as reported for example by Ghergu & Ionescu (2009), Uenishi (2010) and Volkov & Zheltukhin (2015). In particular, inhomogeneous modes whereby consecutive resonant-structures would be in phase-opposition, cannot be excited in the system within the frequency range of interest: They would require a surface motion with a characteristic length of variation $\mathcal{O}(\ell)$ at the dominant order, which is prohibited here due to the scale separation. This kinematic homogeneity also justifies the use of the records from the central accelerometer 1 on the layer top-surface and that at the top of the central resonator A as representative experimental data in the following.

7.2 Site-city effects in the frequency domain

Site-city effects are evidenced in the frequency domain in Fig. 12 for the city configuration 1 with 37 resonators: It shows the transfer functions between the top surface of the layer and the shaking table in both directions X and Y and also that between the top of the central resonator and the shaking table in the resonant direction X. The transfer function $|u_{\text{sheet}}/u_\Gamma|$ of the resonators is also shown. As expected from the CIM (see Section 4.2), soil/city interactions lead to the split of the layer resonant peak in the direction X of city resonance while the layer's transfer function is the usual single peak in the direction Y where the city remains inert. Other phenomena concern the amplitude reduction and the atypical phase in the direction X. These experimental results are in very good agreement (both in amplitude and phase) with the predictions from the CIM and with the numerical results from the BEM (direction X only). Both models are in excellent agreement with one another.

The convolution between the layer top-surface motion and the resonator transfer function in the direction X of resonance (eq. 20 and Figs 12g–h) leads to the resonator's motion shown in Figs 12(e) and (f). The spectrum displays two atypical phenomena compared to that of an isolated resonator on the layer: (1) the resonant peaks correspond neither to the resonator's resonance (eigenfrequency at 8.45 Hz) nor to the layer resonance; and (2) the broadband flat response of the resonator around its eigenfrequency (the city eigenfrequency), has an amplitude $|u_{\text{sheet}}/u_b| = \mathcal{O}(\chi/\eta)$ that can be explained neither by the resonator structural damping ξ nor by the layer's damping ξ_s.

7.3 Site-city effects in the time domain

The unconventional response in the frequency domain gives rise to atypical records in the time domain. To evidence it, Fig. 13 shows the accelerations recorded at the top surface of the layer in the directions X and Y when a Ricker wavelet is prescribed to the shaking table in either of those directions. For comparison, the signals are plotted for the city-configuration 1 with 37 resonators, and for the configuration 5 with a single resonator. In the direction X of city-resonance, the records exhibit lower accelerations and beatings compared to the usual exponentially decreasing oscillations (similarly to that of a layer with a free surface) recorded in the direction X when only a single resonator is present, and in the direction Y, whether with 37 resonators or a single resonator, due to the non-resonant behaviour of those on the direction Y. Signals are synthesized at the layer top-surface with the CIM and the BEM (direction X only) from the Ricker wavelet recorded at the shaking table. Fig. 13 shows that both the theoretical and numerical models describe the site-city effects in the time domain with a good accuracy. Note that the signals synthesized with the CIM in the case of a single resonator on the surface are those of the layer with a free surface: A single resonator does not modify (significantly) the incident field, while the city-arrangement with 37 resonators does.

7.4 Mode shapes

The unconventional features of the layer transfer function in the direction X of city-resonance is associated with specific soil/city mode shapes when a harmonic motion is imposed by the shaking table. Fig. 14 shows those mode shapes at four particular frequencies: out of resonance (5 Hz), at the coupled-soil-city resonance-peaks (around 6.7 Hz and 10 Hz) and at the city-resonance (around 8.4 Hz) close to the eigenfrequency of the layer with a free surface. The mode shapes correspond to the horizontal displacement field in the layer at the time t_0 when the layer experiences the largest displacement. The displacement has been normalized by the amplitude of the harmonic motion prescribed at the shaking table. The displacement of the resonators has been plotted too, using the eigenfunction of a bending beam at its first mode. Out of resonance the behaviour is conventional: for instance at 5 Hz the set-up follows the shaking table in a quasi-static way. At the two coupled soil-city resonance peaks, the layer is at resonance with the usual quarter-wavelength shape while the resonators oscillate in phase (first peak around 6.7 Hz) or in phase opposition (second peak around 10 Hz) with the block. At city-resonance, the surface is nearly stationary while the resonant-structures oscillate. Without the resonant mass of the city, the layer resonance should occur around this frequency. But due to the city-resonance, the surface is a node in the mode shape, as for a rigid surface condition. These experimental results are compared with mode shapes provided by the CIM, eq. (24), and by the BEM (nodal displacement at the free lateral surface of the elastic medium). Both models are in qualitative and quantitative agreement with experimental results and with one another.

7.5 Depolarization

As it has been pointed out in Section 4.1, the anisotropic behaviour of the city leads to atypical depolarization effects, even in a homogeneous medium without topological singularities. Since the city anisotropy induces significant differences between the transfer functions in the directions X and Y (Fig. 12), depolarization can be demonstrated with harmonic motions $\mathbf{U}_b$ (at specific frequencies) prescribed to the shaking table in directions that stand out of the city principal axes X and Y. Figs 15(a)–(e) show the acceleration polarization at the top surface of the layer in response to harmonic excitations applied in the horizontal direction at the angle 45° counted from the direction $\mathbf{e}_X$, for five different frequencies: out of resonance (5 Hz), at the coupled-soil-city resonance-peaks (around 6.7 Hz and 10 Hz) and at the city-resonance (around 8.4 Hz) and at the layer resonance in the Y direction (around 7.3 Hz), close to the city-resonance. Those results evidence that the top surface motion $\mathbf{U}_\Gamma$ can strongly depart from the direction of the input motion $\mathbf{U}_b$.

First, in the frequency range around 8.4 Hz, the response spectrum along X is close to zero due to the city resonance, while the response spectrum along Y is amplified by the resonance of the elastic layer. Consequently the top-surface motion $\mathbf{U}_\Gamma$ is mostly polarized along Y, see Figs 15(c) and (d). Second, in the frequency range around 10 Hz, the response spectrum along X is amplified by the second soil/city coupled
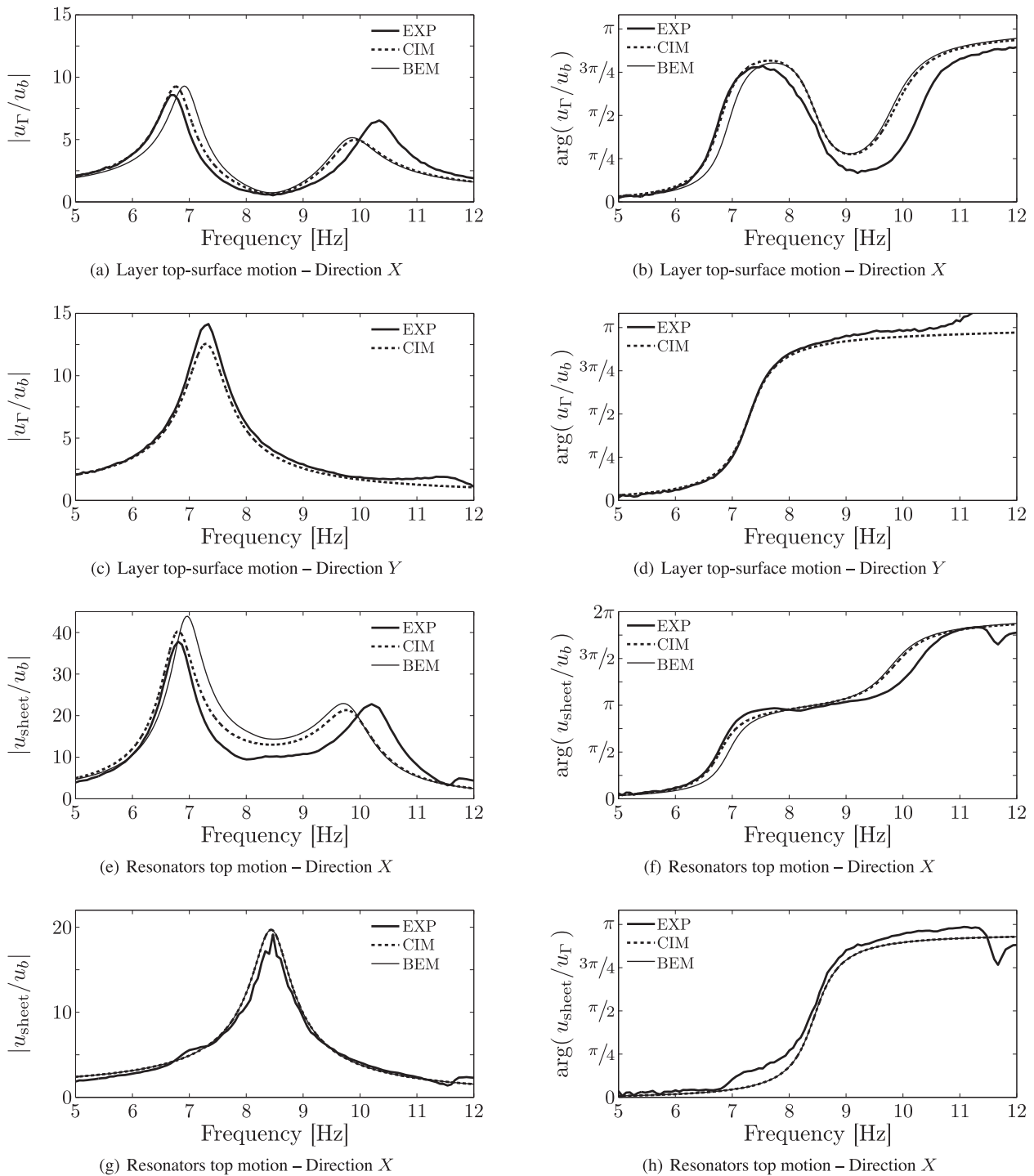
Figure 12. Comparison between the experimental results (EXP), the City-Impedance Model (CIM) and the Boundary Elements Model (BEM) in the frequency domain for the city-configuration 1 with 37 resonators: (a) amplitude and (b) phase of the surface displacement u_Γ in the resonant direction X, normalized by table displacement u_b in that direction; (c) amplitude and (d) phase of the surface displacement u_Γ in the non-resonant direction Y, normalized by table displacement u_b in that direction; (e) amplitude and (f) phase of the displacement u_{sheet} at the top of the resonator in the resonant direction X, normalized by table displacement u_b in that direction; (g) amplitude and (h) phase of the displacement u_{sheet} at the top of the resonator in the resonant direction X, normalized by surface displacement u_Γ in that direction. Experimental data from central accelerometer 1 on the foam block and central resonator A.
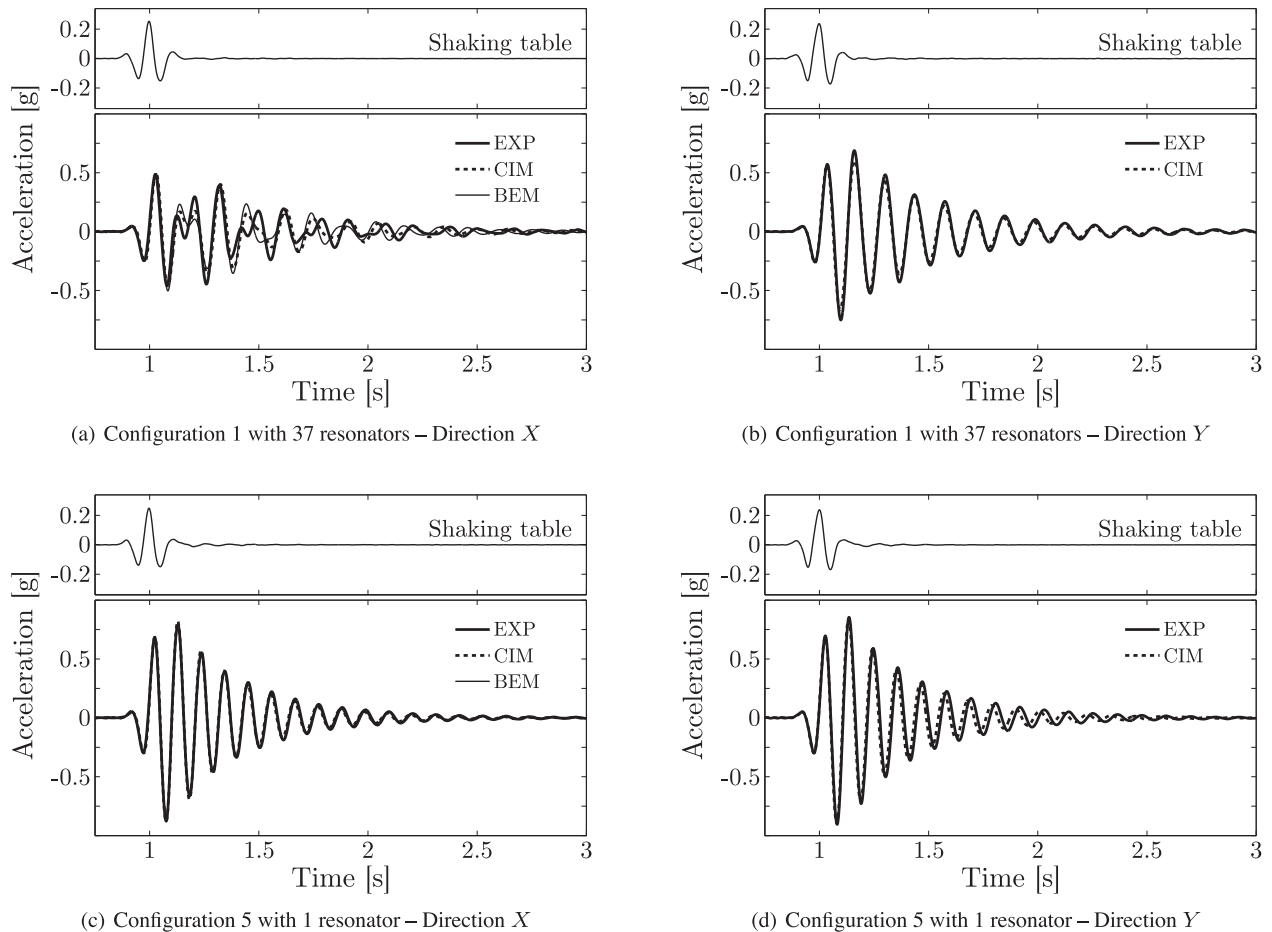
Figure 13. Comparison between the experimental results (EXP), the City-Impedance Model (CIM) and the Boundary Elements Model (BEM) in the time domain: (a, b) for the city-configuration 1 with 37 resonators; (c, d) for the configuration 5 with a single resonator. (a, c) Experimental records (central accelerometer 1) and synthesized signals in the direction X of city-resonance, at the surface of the elastic layer in response to a Ricker wavelet prescribed to the shaking table in the same direction. (b, d) Experimental records (central accelerometer 1) and synthesized signals in the direction Y at the surface of the elastic layer in response to a Ricker wavelet prescribed to the shaking table in the same direction.

resonance, while the response spectrum along Y has passed its resonance and is decreasing. As a result, the top-surface motion $\mathbf{U}_\Gamma$ is mostly polarized along X, see Fig. 15(e). Note that at the first soil/city coupled resonance, the response spectra along X and Y are amplified in a similar way (due to the resonance in the Y direction) but the phase difference between the two principal directions induce an elliptical polarization, see Fig. 15(b). Out of resonance, for example, around 5 Hz, the behaviour is conventional: The top-surface motion $\mathbf{U}_\Gamma$ is polarized linearly in the direction of the shaking table, Fig. 15(a).

All these observations concur with the CIM and evidence that the city can have a substantial effect on the polarization of the seismic field. This is evidenced in the case of a broadband signal in Fig. 15(f) where a Ricker wavelet is applied in the horizontal direction at 45° from the direction X. This polarization can be seen as the combination of the two records given in Fig. 13. What could be regarded at first as an erratic displacement is actually explained by the CIM. Moreover, recall that the shaking table signals is a short impulse: The complex polarization pattern of the surface is the free response of the soil/city system to that impulse.

7.6 City density

The emergence of the Site-city phenomena are studied through a parametric study on the density of the city. For each city configuration represented in Fig. 7, the transfer function between the layer top-surface and the shaking table is plotted in Fig. 16 in both directions X and Y; the transfer function between the displacement at the top of the resonators and the shaking table in the direction X is plotted too, as well as the transfer function between the displacement at the top of the resonators and the layer top-surface.

Fig. 16 shows that, for a given extension of the city, the denser the city, the stronger the effects. In the direction X, the peaks of soil/city coupled resonance are more separated with lower amplitudes as the density increases. Only 5 resonators (configuration 4) are sufficient for the site-city effects to be noticeable in the direction X; the effects are already significant with 9 resonators (configuration 3). In the direction Y, only a decrease in the layer resonance frequency is significant, due to the added inert mass of the city, as explained in Section 4.2.
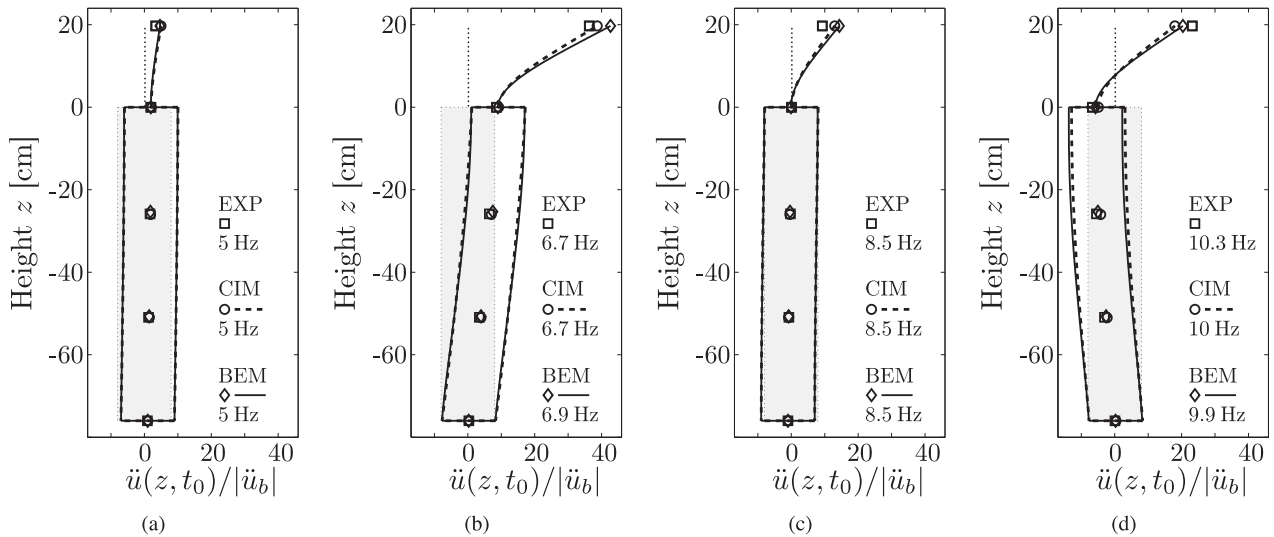
Figure 14. Comparison between the mode shapes from the experimental results (EXP), the City-Impedance Model (CIM) and the Boundary Elements Model (BEM) for the city-configuration 1 with 37 resonators. Deformation profile in the direction X represented on a slab of layer and one resonator: (a) below resonance; (b) at the first soil-city resonance; (c) at the resonance of the city; (d) at the second soil-city resonance. The system without deformation has been represented for reference. Experimental data is obtained in the time domain by central accelerometers 1, 7 and 8 on the foam block and central resonator A, in response to a harmonic motion imposed to the shaking table. The measured accelerations have been normalized by the amplitude of the harmonic input motion and are represented here at the time t_0 when the layer experiences its largest displacement.
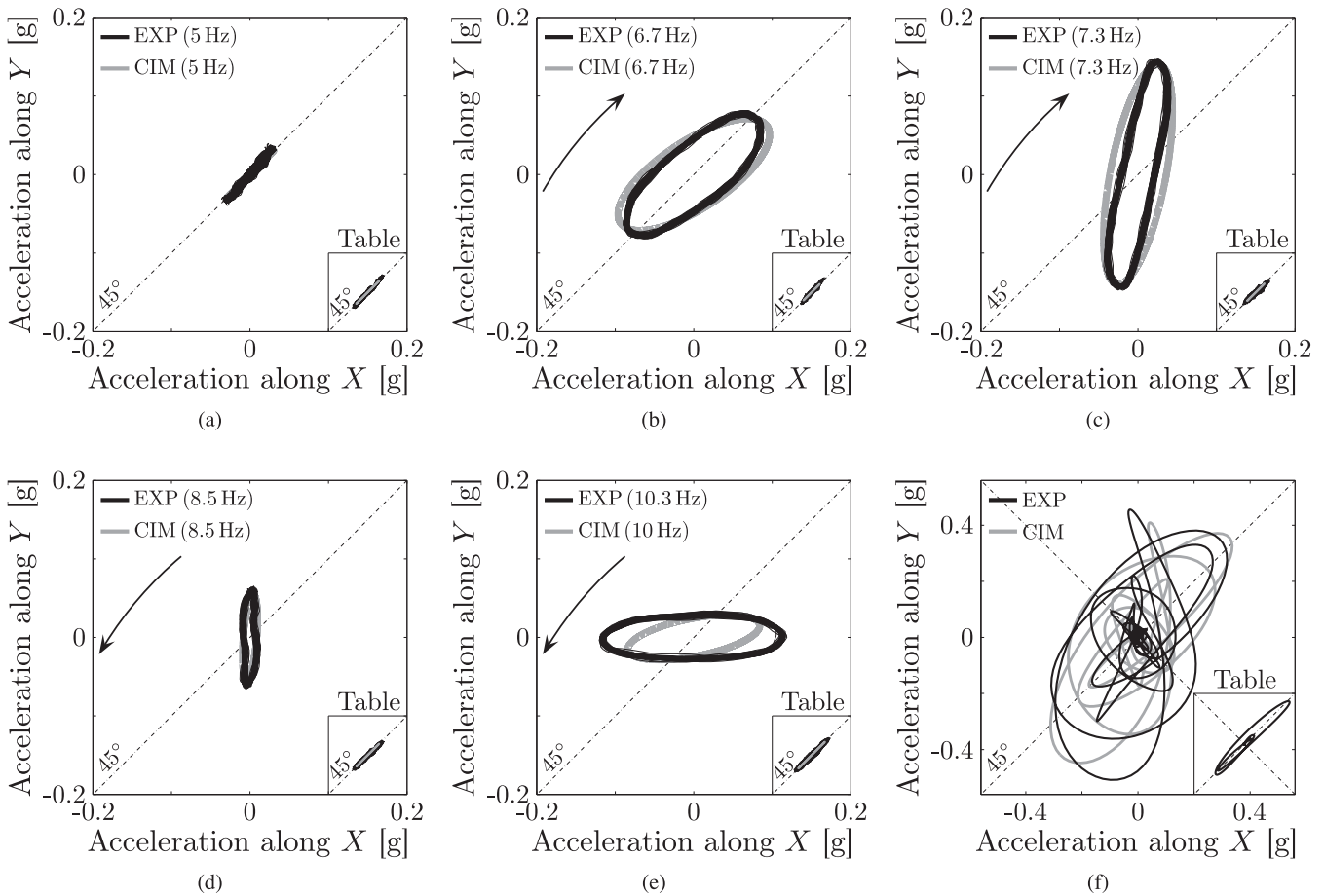

Figure 15. Accelerations recorded at the surface of the foam block (central accelerometers 1) and the shaking table in the directions X and Y for the city-configuration 1 with 37 resonators in response to (a–e) sinusoidal signals with 100 cycles and (f) a Ricker wavelet, prescribed to the shaking table in the 45° direction. Polarization of the particle acceleration represented: (a) below resonance; (b) at the first soil-city resonance in X; (c) at the soil resonance in Y; (d) at the resonance of the city in X; (e) at the second soil-city resonance in X. Comparison with the surface accelerations provided by the City Impedance Model (CIM) in response to similar excitations. The arrow provides the orientation of polarization.
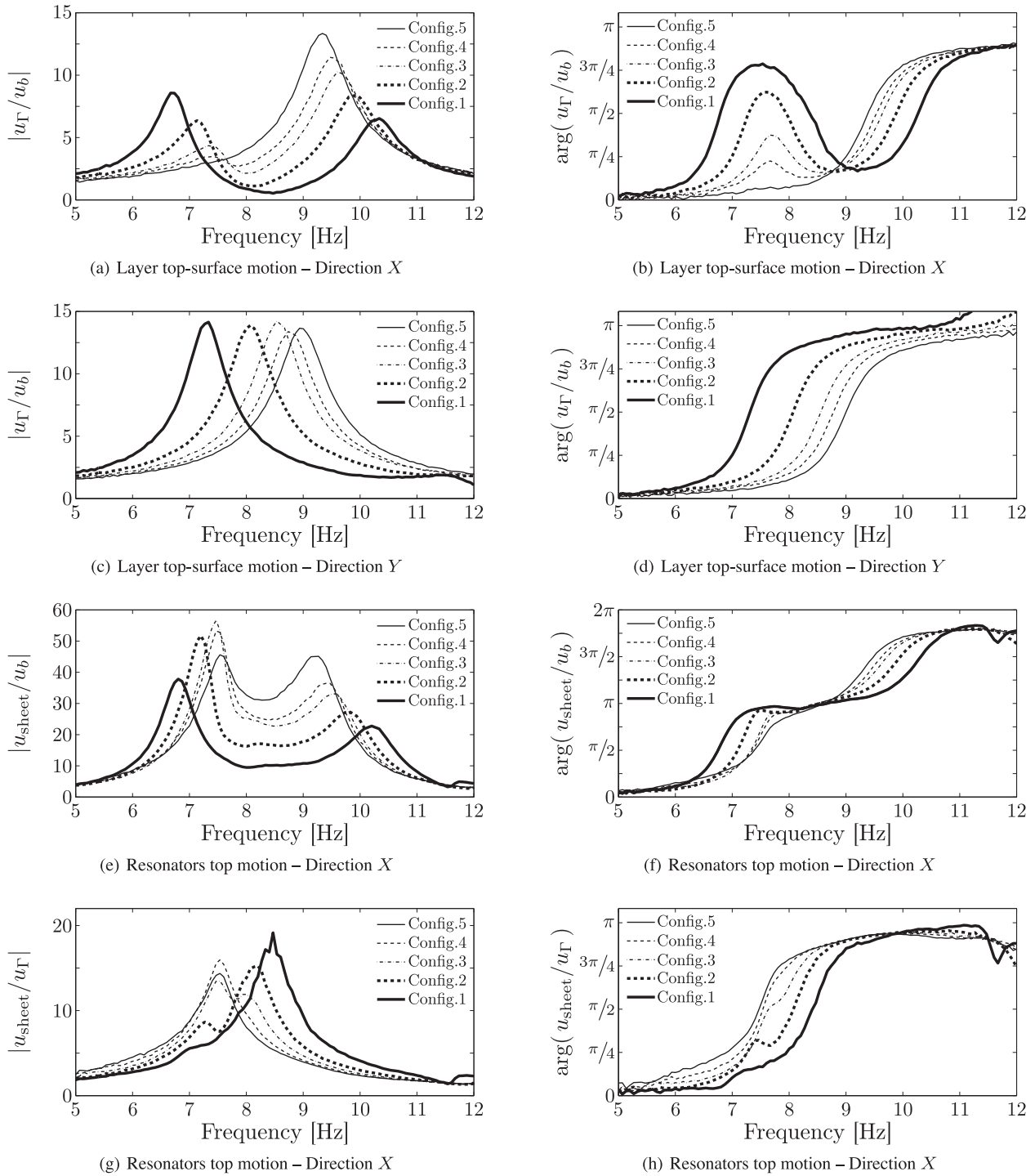
(a) Layer top-surface motion – Direction X

(b) Layer top-surface motion – Direction X

(c) Layer top-surface motion – Direction Y

(d) Layer top-surface motion – Direction Y

(e) Resonators top motion – Direction X

(f) Resonators top motion – Direction X

(g) Resonators top motion – Direction X

(h) Resonators top motion – Direction X

Figure 16. Experimental transfer functions for the city-configurations 1 to 5 with 37, 19, 9, 5 and 1 resonators respectively: (a) amplitude and (b) phase of the surface displacement u_Γ in the resonant direction X, normalized by table displacement u_b in that direction; (c) amplitude and (d) phase of the surface displacement u_Γ in the non-resonant direction Y, normalized by table displacement u_b in that direction; (e) amplitude and (f) phase of the displacement u_{sheet} at the top of the resonator in the resonant direction X, normalized by table displacement u_b in that direction; (g) amplitude and (h) phase of the displacement u_{sheet} at the top of the resonator in the resonant direction X, normalized by surface displacement u_Γ in that direction. Experimental data from central accelerometer 1 on the foam block and central resonator A.

Another significant phenomenon is the resonance frequency shift and split observed in Figs 16(g)–(h), with transitional configurations 2 and 3 being of particular interest. Indeed, as the city-density increases, the apparent resonance frequency of the city increases too. This is due to a reduction of the boundary layer flexibility under the foundations as the city gets denser, see eq. (16), in particular that regarding the rotation of the foundations. Models can be proposed to quantify that effect (Schwan 2014) but they are out of the scope of this paper. Instead, as it has been explained in Section 6.1, the eigenfrequency of the resonators has been matched with that observed experimentally for each city-configuration in the CIM and the BEM. Recall that the city-configurations satisfy all the elementary properties of the theoretical model for site-city interactions (periodicity, extension over the whole surface of the layer) but the condition of a sharp scale separation (except the configuration with 37 resonators). The CIM is applied nevertheless and its results are compared with the experimental and numerical results: Fig. 17 shows the transfer functions of the layer thus obtained in the direction X of city-resonance. The CIM remains accurate both qualitatively and quantitatively even for large periods Σ: In practice, the physical concepts underlying the phenomena under the long-wavelength approximation are still pertinent under poor scale separations. The BEM is in good agreement with both the experimental results and the CIM.

7.7 Discussion

Numerical and experimental validation of the CIM. The good agreement observed in Figs 10 to 17 between the analytical, experimental and numerical results in the cross-section XZ and between the analytical and experimental models in the 3-D in general, validates the CIM and clearly evidences the signatures of site-city effects predicted by the theory. To simplify the demonstration, the study has been focused experimentally on plane shear waves. However, the presented CIM applies for wavefields of any kind, provided that the scale separation is satisfied. Furthermore, to comply as closely as possible with the basic assumptions of homogenization, periodic arrangements of resonators have been considered. Note however that when the scale separation is sharp, periodic or non-periodic spatial distribution lead to similar macroscopic behaviour (Auriault *et al.* 2009). This idea is supported by a large range of complementary parametric experiments (Schwan 2014) that show the robustness of the concept of city-impedance and the possibility to combine phenomena related to different resonator arrays (which would make the subject of another article). Recall however that the notion of effective impedance relies on the existence of a scale separation under the long-wavelength approximation; other phenomena can occur at high frequencies, as presented for instance by Ghergu & Ionescu (2009); Uenishi (2013); and Volkov & Zheltukhin (2015).

Moreover, the theoretical CIM is, in essence, 3-D. This particularity allowed Boutin & Roussillon (2006) to predict the depolarization of elastic waves by anisotropic structures: Such depolarization effects necessarily require a 3-D model to be explained. In order to evidence clearly those depolarization effects, the present study has been focused experimentally on strongly anisotropic structures. This strong anisotropy allowed the application of a 2-D boundary element formulation in order to study the system in the cross-section XZ. In that plane, the numerical, analytical and experimental models are comparable and a very good agreement is observed between them. However, the 2-D numerical model is limited to the cross-section XZ and cannot account for the depolarization.

Make models comparable. The present study aimed at isolating the site-city interactions in a well-controlled idealized environment in order to discriminate and characterize the phenomena of multiple SSSIs. In particular, the analytical formulation of the CIM enabled the design of an analogous prototype, wherein attention has been paid for the experimental and numerical models to share a common set of properties with the theoretical model, so that the three of them are comparable. One particular aspect of it lies in the boundary conditions applied in the experimental model (paragraph 5.1) and numerical model (paragraph 6.1) so that the theoretical horizontal kinematic of a layer (with infinite lateral extension) is recovered for the elastic block without the city for every model (e.g. see Figs 17a and b for the response of the layer top-surface with a single resonator). That involves restraining the vertical motion with edge rods in the experimental model, and preventing it near the edges at the block top-surface in the numerical model. Despite the good agreement between the models, some minor discrepancies can be found in Figs 12 and 17, in particular regarding the frequency of the second resonance peak in the direction X in the presence of the resonators. Moreover, the differences between the analytical (CIM) and numerical (BEM) models remain small for all city-configurations, while they are more significant between these two and the experimental results. At this stage, several hypotheses can be formulated to explain those discrepancies, which would require further analyses: The inherent dispersion of the resonators' modal properties in the experimental realization which could widen the frequency range of the city-resonance; the reduction of the resonators' behaviour to a mass-spring oscillator in the theoretical and numerical models (moments of inertia are neglected); the effects of the correctors in the asymptotic approach, and in particular the effects of the rocking of the foundations; the boundary conditions applied to the elastic medium, which differ in the way stresses are balanced near the edges; and numerical approximations associated with the discretization performed in the boundary element model. Besides, the limited expression of additional kinematics of the elastic block at higher frequencies (around 11.5 Hz) can also be noted in Fig. 16, which are not accounted for in the models.

Example of handy application. The analytical model provides the key parameters (scale parameter at resonance ε_o; the parameter η; and the buildings' damping $\xi \ll 1$) that can be used as indicators to help find building arrangements which favour multiple SSSIs in urban landscapes or industrial plants. This idea is illustrated by considering a group of identical nearby-buildings, the characteristics of which are taken from Hans *et al.* (2005): they are 43.2 m high (15 storeys), 31.4 m long and 13.4 m wide, with the linear mass 110 t/m in height, the eigenfrequency 1.56 Hz and the damping $\xi = 1.5$ per cent. The buildings are supposed to be separated by a 10 m wide gap (period $\Sigma = \ell \times L$, with $\ell = 23.4$ m and $L = 41.4$ m) and to be built on a soil with the density and shear-wave velocity of the order $\rho \sim 1800$ kg m^{-3} and
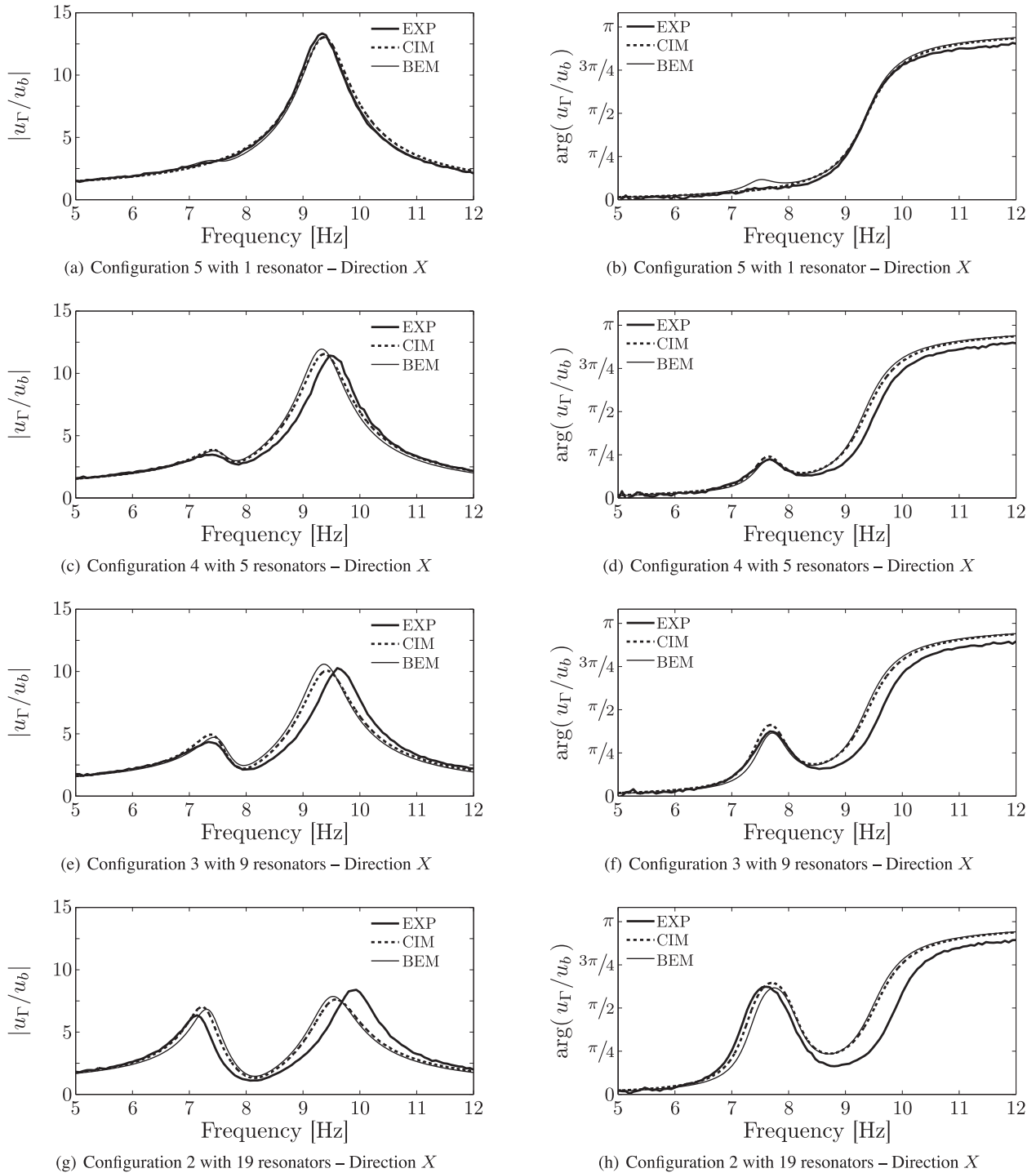
Figure 17. Amplitude (left) and phase (right) against frequency of the surface displacement u_Γ in the resonant direction X, normalized by the table displacement u_b in that direction. Comparison between the experimental results (EXP), the City-Impedance Model (CIM) and the Boundary Elements Model (BEM): (a, b) city-configuration 5 with 1 resonator; (c, d) city-configuration 4 with 5 resonators; (e, f) city-configuration 3 with 9 resonators; (g, h) city-configuration 2 with 19 resonators. Experimental data from central accelerometer 1 on the foam block.

$c_s \sim 250\,\mathrm{m\,s^{-1}}$. The key parameters take the values: $\varepsilon_o = \ell\omega_o/c_s \approx 0.88 < 1$ and $\eta = m_o\omega_o/(|\Sigma|\rho c_s) \approx 10\,$per cent. The scale parameter ε_o suggests that the impedance model can be applied (despite a poor scale separation) while the ratio $\eta/2\xi \approx 3$ suggests significant multibuilding interactions.

Comparison with other studies. The same procedure can be applied to configurations considered in other studies. For example, Kham *et al.* (2006) analysed numerically, by means of a 2-D boundary element method, the effect of up to 33 building-like blocks arranged periodically at the surface of an elastic basin over a distance of 500 m (building spacing is around 15 m). They showed that a group effect among the buildings led to a ground motion reduction which was enhanced by higher densities. Those numerical observations are similar to

those obtained in the present paper. Actually, with a frequency range below 2 Hz and a shear-wave velocity around $200\,\mathrm{m\,s^{-1}}$, the scale factor is below 0.95 in this case, which suggests that the CIM could be applied in that configuration. The interaction parameter $\eta \sim 17$ per cent assessed from the material properties found in their article, associated with the building damping $\xi = 5$ per cent leads to $\eta/(2\xi) \sim 1.7$ which indicates significant interactions, as testified by their numerical simulations.

Another example is given by Isbiliroglu *et al.* (2015) who analysed, by means of sophisticated finite element techniques, the 3-D response of up to $9 \times 9 = 81$ isotropic building-like blocks arranged periodically in a square pattern at the surface of a realistic geological stratification. The presence of a double peak can be observed in the spectrum of the motion at the top of the buildings. Moreover, little variability can be observed in the response spectra from one building to another in the low frequency range. That probably bears testament to similar group effects than those studied in the present study, despite the complex geological structures. In fact, in the frequency range around 1 Hz, for shear-wave velocity around $300\,\mathrm{m\,s^{-1}}$ and with building spacings of 20 m to 40 m, the scale parameter ranges from 0.42 to 0.84 approximately, which suggests once again that the CIM could be applied in that configuration to analyse those phenomena.

On the other hand, the 2-D situations described by Tsogka & Wirgin (2003), extended by Groby *et al.* (2005) for viscoelasticity, and the wide range of city configurations described by Groby & Wirgin (2008), do not seem within the scope of the present CIM. In those studies, the city is settled on 50 m thick soft soil layer (shear-wave velocity $c_1 = 60\,\mathrm{m\,s^{-1}}$), resting on a half-space bedrock (shear-wave velocity $c_2 = 600\,\mathrm{m\,s^{-1}}$). For building-spacings $\ell \geq 60$ m and a frequency range around $\omega/(2\pi) \sim 0.5$ Hz, the scale parameter in the soft layer is $\ell\omega/c_1 \geq 3$. These configurations are far beyond the scale separation that the CIM requires.

8 CONCLUSIONS

The specificity of the present study lies in the coincidence within the same frequency range of a long-wavelength dynamics in the soil layer, and the local resonance of the buildings. The surface resonance then leads to particular boundary conditions expressed through asymptotic homogenization in terms of a frequency-dependent impedance matrix (potentially anisotropic). This phenomenon and its formulation depart from the usual conditions of a free surface: The collective behaviour of city buildings can differ greatly from that expected from conventional seismic analyses.

The fact that a city group effect can notably modify the seismic response of both the implantation site and the constitutive buildings has been demonstrated experimentally, theoretically and numerically, with a systematic comparison between the three approaches. The particular methodology made sure that the three of them are based on the same set of basic properties regarding the soil behaviour (linear elasticity), the building models (SDOF oscillator), the city model (periodic arrangement of similar buildings), the frequency range of investigation (city/layer co-resonance under scale separation) and the nature of the excitation. This study brings basic experimental data that clearly evidence a site-city effect issued from up to 37 resonators arranged at the top of an elastic layer. Signatures of site-city interactions have been identified and include in particular: Split resonance peaks in layer responses; beatings in records; and atypical (de)polarization of the surface motion in the presence of anisotropic resonant structures. Site-city effects can be noticeable with as few as five structures.

The main interest of the CIM relies on the two following facts: (1) it pares the complexity of multibuilding interactions down to its most crucial characteristics described explicitly in an analytical formulation issued from the fundamental principles of elastodynamics; and (2) it allows the 3-D calculations at very low computation cost, particularly well adapted for preliminary analysis. Moreover, the complex SSSIs at the city scale and the expected accuracy of the description are quantified by three parameters: The scale parameter at resonance ε_o; the parameter η related to the impedance contrast between the city and the soil; and the damping $\xi \ll 1$ of the buildings. They are a-priori indicators which can be assessed before any sophisticated simulations.

Certainly, the experimental setup considered here is quite far from the complexity of realistic geological sites and cities in many respects; but it should be considered as a proof of concept for multistructure interactions among a large group of buildings. The next step would be to bring these concepts in the field and identify site-city signatures in in-situ records. Once again, to help find favourable building arrangements in urban landscapes or industrial plants, the aforementioned indicators can be assessed.

REFERENCES

Adeline, K.R.M., Chen, M., Briottet, X., Pang, S.K. & Paparoditis, N., 2013. Shadow detection in very high spatial resolution aerial images: a comparative study, *ISPRS J. Photogramm. Remote Sens.,* **80,** 21–38.

Auriault, J.-L., Boutin, C. & Geindreau, C., 2009. *Homogenization of Coupled Phenomena in Heterogenous Media,* ISTE.

Bonnefoy-Claudet, S., Baize, S., Bonilla, L.F., Berge-Thierry, C., Pasten, C., Campos, J., Volant, P. & Verdugo, R., 2008. Site effect evaluation in the basin of santiago de chile using ambient noise measurements, *Geophys. J. Int.,* **176**(3), 925–937.

Boutin, C. & Roussillon, P., 2004. Assessment of the urbanization effect on seismic response, *Bull. seism. Soc. Am.,* **94**(1), 251–268.

Boutin, C. & Roussillon, P., 2006. Wave propagation in presence of oscillators on the free surface, *Int. J. Eng. Sci.,* **44,** 180–204.

Boutin, C., Schwan, L. & Dietz, M. S., 2015. Elastodynamic metasurface: Depolarization of mechanical waves and time effect, *J. Appl. Phys.,* **117,** 064902, doi:10.1063/1.4908135.

Castellaro, S. & Mulargia, F., 2010. How far from a building does the ground-motion free-field start? the cases of three famous towers and a modern building, *Bull. seism. Soc. Am.,* **100**(5A), 2080–2094.

Chávez-García, F.J. & Bard, P.-Y., 1994. Site effects in Mexico City eight years after the September 1985 Michoacan earthquakes, *Soil Dyn. Earthq. Eng.,* **13**, 229–247.

Chávez-García, F.J. & Cárdenas-Soto, M., 2002. The contribution of the built environment to the "free field" ground motion in Mexico City, *Soil Dyn. Earthq. Eng.,* **22**, 773–780.

Chazelas, J.-L., Gueguen, P., Bard, P.-Y. & Semblat, J.-F., 2003. Modélisation de l'effet site-ville en modèle réduit centrifugé. validation des technques expérimentales, in *6eme Colloque National de Génie Parasismique. Ecole Polytechnique, Palaiseau, France,* vol. 1, pp. 245–252.

Clouteau, D. & Aubry, D., 2001. Modification of ground motion in dense urban areas, *J. Comput. Acoust.,* **9**(4), 1659–1675.

Domínguez, J., 1993. *Boundary Elements in Dynamics,* Computational Mechanics Publications and Elsevier Applied Science.

Figueiredo, L. & Amorim, L., 2007. Decoding the urban grid : or why cities are neither trees nor perfect grids, in *Proceedings of the 6th International Space Syntax Symposium, Istanbul,* eds Kubat, A.S., Ertekin, O., Guney, Y.I. & Eyuboglu, E., ITU Faculty of Architectur, Istanbul, Turkey.

Ghergu, M. & Ionescu, I.R., 2009. Structure-soil-structure coupling in seismic excitation and "city effect", *Int. J. Eng. Sci.,* **47**, 342–354.

Groby, J.-P. & Wirgin, A., 2008. Seismic motion in urban site consisting of blocks in welded contact with a soft layer overlying a hard half-space, *Geophys. J. Int.,* **172**(2), 725–758.

Groby, J.-P., Tsogka, C. & Wirgin, A., 2005. Simulation of seismic response in a city-like environment, *Soil Dyn. Earthq. Eng.,* **25**, 487–504.

Guéguen, P., Bard, P.-Y. & Chávez-García, F.J., 2002. Site-city seismic interaction in Mexico City-like environments: an analytical study, *Bull. seism. Soc. Am.,* **92**(2), 794–811.

Hans, S., Boutin, C., Ibraim, E. & Roussillon, P., 2005. In situ experiments and seismic analysis of existing buildings. Part I: Experimental investigations, *Earthq. Eng. Struct. Dyn.,* **34**, 1513–1529.

Hartog, J.P.D., 1956. *Mechanical Vibrations,* Dover.

Holloway, C.L. & Kuester, E.F., 2000. Equivalent boundary conditions for a perfectly conducting periodic surface with a cover layer, *Radio Sci.,* **35**(3), 661–681.

Isbiliroglu, Y., Taborda, R. & Bielak, J., 2015. Coupled soil-structure interaction effects of building clusters during earthquakes, *Earthq. Spectra,* **31**(1), 463–500.

Jennings, P.C., 1970. Distant motion from a building vibration test, *Bull. seism. Soc. Am.,* **60**(6), 2037–2043.

Jennings, P.C. & Bielak, J., 1973. Dynamics of building-soil interaction, *Bull. seism. Soc. Am.,* **63**(1), 9–48.

Kham, M., Semblat, J.-F., Bard, P.-Y. & Dangla, P., 2006. Seismic site-city interaction: main governing phenomena through simplified numerical model, *Bull. seism. Soc. Am.,* **96**(5), 1934–1951.

Kitada, Y., Hirotani, T. & Iguchi, M., 1999. Model test on dynamic structure-structure interaction of nuclear power plant buildings, *Nucl. Eng. Des.,* **192**, 205–216.

Luco, J. E. & Contesse, L., 1973. Dynamic structure-soil-structure interaction, *Bull. seism. Soc. Am.,* **63**(4), 1289–1303.

Padrón, L.A., Maeso, O. & Aznárez, J.J., 2004. Cálculo de estructuras de barras incluyendo efectos dinámicos de interacción suelo-estructura. Modelo mixto de elementos finitos y elementos de contorno, *Master's thesis,* Universidad de Las Palmas de Gran Canaria, Spain, (http://hdl.handle.net/10553/10472, in Spanish).

Padrón, L.A., Aznárez, J.-J. & Maeso, O., 2009. Dynamic structure-soil-structure interaction between nearly piled building under seismic excitation by BEM-FEM model, *Soil Dyn. Earthq. Eng.,* **29**, 1084–1096.

Sánchez-Palencia, E., 1980. *Non-homogeneous Media and Vibration Theory,* vol. 127 of Lecture Notes in Physics, Springer-Verlag.

Schwan, L., 2014. Étude théorique et expérimental de surfaces résonante en milieu élastique: Application à l'effet site-ville et la conception de métasurfaces, *PhD thesis,* E.N.T.P.E., Université de Lyon, France.

Schwan, L. & Boutin, C., 2013. Unconventional wave reflection due to "resonant surface", *Wave Motion,* **50**, 852–868.

Semblat, J.-F., Kham, M. & Bard, P.-Y., 2008. Seismic-wave propagation in alluvial basins and influence of site-city interaction, *Bull. seism. Soc. Am.,* **98**(6), 2665–2678.

Sieffert, J.-G. & Cevaer, F., 1992. *Handbook of Impedance Functions,* Ouest Editions.

Singh, S. K. & Ordaz, M., 1993. On the origin of long coda observed in the lake-bed strong-motion records of Mexico City, *Bull. seism. Soc. Am.,* **83**(4), 1298–1306.

Sohn, G. & Dowman, I., 2007. Data fusion of high resolution satellite imagery and LiDAR data for automatic building extraction, *ISPRS J. Photogramm. Remote Sens.,* **62**, 43–63.

Taborda, R. & Bielak, J., 2011. Full 3D integration of site-city effects in regional scale earthquake simulations, in *Proceedings of 8th International Conference on Structural Dynamics, Eurodyn,* pp. 511–518, eds De Roeck, G., Degrande, G., Lombaert, G. & Müller, G., Leuven, Belgium.

Tsogka, C. & Wirgin, A., 2003. Simulation of seismic response in an idealized city, *Soil Dyn. Earthq. Eng.,* **23**, 391–402.

Uenishi, K., 2010. The city effect: dynamic interaction between a group of structures and waves in the ground, *Rock Mech. Rock Eng.,* **43**(6), 811–819.

Uenishi, K., 2013. "Unexpected" failure patterns and dynamic collective behaviour of an assembly of buildings subjected to horizontal impact, *Eng. Failure Anal.,* **35**, 125–132.

Volkov, D. & Zheltukhin, S., 2015. Preferred frequencies for coupling of seismic waves and vibrating tall buildings, *Soil Dyn. Earthq. Eng.,* **74**, 25–39.

Wirgin, A. & Bard, P.-Y., 1996. Effects of building on the duration and amplitude of ground motion in Mexico City, *Bull. seism. Soc. Am.,* **86**(3), 914–920.

Wolf, J. P., 1994. *Foundation Vibration Analysis using Simple Physical Models,* Prentice Hall, Inc.

Wong, H. & Trifunac, M., 1975. Two-dimensionnal, antiplane, building-soil-building interaction for two or more buildings and for incident plane SH waves, *Bull. seism. Soc. Am.,* **65**(6), 1863–1885.

Yoshida, H. & Omae, M., 2005. An approach for analysis of urban morphology: methods to derive morphological properties of city blocks by using an urban landscape model and their interpretations, *Comput. Environ. Urban Syst.,* **29**, 223–247.

APPENDIX: TWO-SCALE ASYMPTOTIC HOMOGENIZATION OF THE CITY

Following the homogenization method (Sánchez-Palencia 1980; Auriault *et al.* 2009), the fields are expanded in power of $\varepsilon \ll 1$ (orders are specified in superscripts) such as

$$\mathbf{u}(\mathbf{x}) = \mathbf{u}^{(0)}(\mathbf{x}) + \varepsilon \mathbf{u}^{(1)}(\mathbf{x}, \mathbf{y}) + \ldots; \tag{A1}$$

$$\sigma^\star(\mathbf{x}_\Gamma, \mathbf{y}) = \sigma^{\star(0)}(\mathbf{x}_\Gamma, \mathbf{y}) + \varepsilon \sigma^{\star(0)}(\mathbf{x}_\Gamma, \mathbf{y}) + \ldots; \tag{A2}$$

and similarly for the fields $\sigma(\mathbf{x})$, $\mathbf{F}(\mathbf{x}_\Gamma)$, $\mathbf{M}(\mathbf{x}_\Gamma)$, $\mathbf{t}(\mathbf{x}_\Gamma, \mathbf{y})$, $\mathbf{u}_S$ and θ_S. In accordance with the BL estimate in eq. (12), the expansion of $\mathbf{u}^\star(\mathbf{x}_\Gamma, \mathbf{y})$ begins at the order ε:

$$\mathbf{u}^\star(\mathbf{x}_\Gamma, \mathbf{y}) = \varepsilon \mathbf{u}^{\star(1)}(\mathbf{x}_\Gamma, \mathbf{y}) + \dots. \tag{A3}$$

The expansions are introduced in eqs (4)–(9). Terms of equal power of ε are collected, providing problems that are solved in increasing order of ε-powers. At the order ε^0, the following holds:

$$\sigma^{\star(0)} = \mathbf{C} : \mathbf{e}_y(\mathbf{u}^{\star(1)}); \tag{A4a}$$

$$\mathbf{div}_y \sigma^{\star(0)} = \mathbf{0}; \tag{A4b}$$

$$[\sigma^{(0)} + \sigma^{\star(0)}].\mathbf{n} = \mathbf{t}^{(0)}(\mathbf{x}_\Gamma, \mathbf{y}_\Gamma); \tag{A4c}$$

$$\int_S \mathbf{t}^{(0)} \, dS_y = \mathbf{F}^{(0)}; \tag{A4d}$$

$$\int_S (\mathbf{y} - \mathbf{y}_S) \wedge \mathbf{t}^{(0)} \, dS_y = \mathbf{M}^{(0)}; \tag{A4e}$$

$$\mathbf{t}^{(0)} = \mathbf{0} \quad \text{on } \Sigma \backslash S; \tag{A4f}$$

$$\mathbf{u}_S^{(0)} = \mathbf{u}^{(0)}; \tag{A4g}$$

$$\mathbf{u}^{\star(1)} = \mathbf{u}_S^{\star(1)} + \theta_S^{(0)} \wedge (\mathbf{y} - \mathbf{y}_S) \quad \text{at S;} \tag{A4h}$$

$$\sigma^{\star(0)}.\mathbf{n} \to \mathbf{0} \quad \text{and} \quad \mathbf{u}^{\star(1)} \to \mathbf{0} \quad \text{as } |\mathbf{y} \cdot \mathbf{n}| \to \infty. \tag{A4i}$$

The absence of inertial term in eq. (A4b) shows that the boundary layer equilibrium is quasi-static at the leading order. It indicates that the boundary layer has a thickness $\mathcal{O}(\ell) \ll \Lambda$. Applying the divergence theorem and using the Σ-periodicity and evanescence of $\sigma^{\star(0)}$, the integration of (A4b) over the column Ω of medium normal to one period Σ (see Fig. 2) leads to

$$\int_\Omega \mathbf{div}_y \sigma^{\star(0)} \, d\Omega_y = \int_\Sigma \sigma^{\star(0)}.\mathbf{n} \, d\Sigma_y = \mathbf{0}. \tag{A5}$$

Since the stress field $\sigma^{(0)}(\mathbf{x})$ is uniform on Σ (area $|\Sigma|$):

$$\int_\Sigma \sigma^{(0)}.\mathbf{n} \, d\Sigma_y = |\Sigma| \sigma^{(0)}.\mathbf{n}. \tag{A6}$$

Besides, using eqs (A4d) and (A4f), the integration of the stress $\mathbf{t}^{(0)}$ over the period Σ yields:

$$\int_\Sigma \mathbf{t}^{(0)} \, d\Sigma_y = \int_{\Sigma \backslash S} \mathbf{t}^{(0)} \, d\Sigma_y + \int_S \mathbf{t}^{(0)} \, dS_y = \mathbf{0} + \mathbf{F}^{(0)}. \tag{A7}$$

Finally, integration of eq. (A4c) over the period Σ gives

$$\int_\Sigma \sigma^{\star(0)}.\mathbf{n} \, d\Sigma_y + \int_\Sigma \sigma^{(0)}.\mathbf{n} \, d\Sigma_y = \int_\Sigma \mathbf{t}^{(0)} \, d\Sigma_y. \tag{A8}$$

Combining eqs (A5)–(A8), the effective boundary condition is derived for the long-wavelength field:

$$\sigma^{(0)}.\mathbf{n} = \mathbf{F}^{(0)}/|\Sigma| \quad \text{on } \Gamma. \tag{A9}$$

As seen in Section 3.4, this condition is sufficient for a leading order description of the long-wavelength field. For a more accurate description, the BL displacement at the foundation can be accounted for. In that aim, consider a test field $\hat{\mathbf{u}}$; using eq. (A4a), periodicity and evanescence of the BL fields, the weak form of eq. (A4b) reads:

$$\int_\Omega \mathbf{e}_y(\hat{\mathbf{u}}) : \mathbf{C} : \mathbf{e}_y(\mathbf{u}^{\star(1)}) \, d\Omega_y = \int_\Sigma \hat{\mathbf{u}} \cdot (\mathbf{t}^{(0)} - \sigma^{(0)}.\mathbf{n}) \, d\Sigma_y. \tag{A10}$$

Since $\hat{\mathbf{u}}$ satisfies the rigid-body motion of the foundation:

$$\hat{\mathbf{u}} = \hat{\mathbf{u}}_S + \hat{\theta} \wedge (\mathbf{y} - \mathbf{y}_S) \quad \text{at } S, \tag{A11}$$

and using the boundary conditions (A4d), (A4f) and (A9), eq. (A10) can be re-written as

$$\int_\Omega \mathbf{e}_y(\hat{\mathbf{u}}) : \mathbf{C} : \mathbf{e}_y(\mathbf{u}^{\star(1)}) \, d\Omega_y = (\hat{\mathbf{u}}_S - \langle \hat{\mathbf{u}} \rangle) \cdot \mathbf{F}^{(0)} + \hat{\theta} \cdot \mathbf{M}^{(0)}, \tag{A12}$$

where $\langle \hat{\mathbf{u}} \rangle = |\Sigma|^{-1} \int_{\Sigma} \hat{\mathbf{u}} d\Sigma_{\mathbf{y}}$ is the mean value of $\hat{\mathbf{u}}$ over the period Σ. Eq. (A12) shows that the energy of elastic deformation results from the work of the force $\mathbf{F}^{(0)}$ and moment $\mathbf{M}^{(0)}$ within BL foundation kinematics. The problem being linear with $\mathbf{F}^{(0)}$ and $\mathbf{M}^{(0)}$ as independent source terms, the BL field $\mathbf{u}^{\star(1)}$ takes the following form:

$$\mathbf{u}^{\star(1)} = \mathbf{a}^{\star(1)} . \mathbf{F}^{(0)} + \mathbf{b}^{\star(1)} . \mathbf{M}^{(0)}, \tag{A13}$$

where $\mathbf{a}^{\star(1)} = \sum_j \mathbf{e}_j \otimes \mathbf{a}_j^{\star(1)}$ and $\mathbf{b}^{\star(1)} = \sum_j \mathbf{e}_j \otimes \mathbf{b}_j^{\star(1)}$ are matrices, the column vectors $\mathbf{a}_j^{\star(1)}$ and $\mathbf{b}_j^{\star(1)}$ of which are defined as the unique solutions of eq. (A12) for unit forces $\mathbf{F}^{(0)}$ and moments $\mathbf{M}^{(0)}$ applied in the direction $\mathbf{e}_j$, respectively:

$$\int_{\Omega} \mathbf{e}_{\mathbf{y}}(\hat{\mathbf{u}}) : \mathbf{C} : \mathbf{e}_{\mathbf{y}} \left(\mathbf{a}_j^{\star(1)} \right) d\Omega_{\mathbf{y}} = (\hat{\mathbf{u}}_S - \langle \hat{\mathbf{u}} \rangle) \cdot \mathbf{e}_j; \tag{A14a}$$

$$\int_{\Omega} \mathbf{e}_{\mathbf{y}}(\hat{\mathbf{u}}) : \mathbf{C} : \mathbf{e}_{\mathbf{y}} \left(\mathbf{b}_j^{\star(1)} \right) d\Omega_{\mathbf{y}} = \hat{\theta} \cdot \mathbf{e}_j. \tag{A14b}$$

Using the BL field itself as the test field, that is, $\hat{\mathbf{u}} = \mathbf{u}^{\star(1)}$, in these last equations, the BL translation $\mathbf{u}_S^{\star(1)} - \langle \mathbf{u}^{\star(1)} \rangle$ of the foundation and its rotation θ_S are found in the form:

$$\mathbf{u}_S^{\star(1)} - \langle \mathbf{u}^{\star(1)} \rangle = \mathcal{S}_t^{\star(1)} . \mathbf{F}^{(0)} + \mathcal{S}_c^{\star(1)} . \mathbf{M}^{(0)}; \tag{A15a}$$

$$\theta_S = \mathcal{S}_c^{\star(1)} . \mathbf{F}^{(0)} + \mathcal{S}_r^{\star(1)} . \mathbf{M}^{(0)}; \tag{A15b}$$

where the components (j, k) of the symmetric matrices of flexibility $\mathcal{S}_t^{\star(1)}$, $\mathcal{S}_c^{\star(1)}$ and $\mathcal{S}_r^{\star(1)}$ read:

$$\mathcal{S}_t^{\star(1)} \Big|_{jk} = \int_{\Omega} \mathbf{e}_{\mathbf{y}} \left(\mathbf{a}_k^{\star(1)} \right) : \mathbf{C} : \mathbf{e}_{\mathbf{y}} \left(\mathbf{a}_j^{\star(1)} \right) d\Omega_{\mathbf{y}}; \tag{A16a}$$

$$\mathcal{S}_c^{\star(1)} \Big|_{jk} = \int_{\Omega} \mathbf{e}_{\mathbf{y}} \left(\mathbf{a}_k^{\star(1)} \right) : \mathbf{C} : \mathbf{e}_{\mathbf{y}} \left(\mathbf{b}_j^{\star(1)} \right) d\Omega_{\mathbf{y}}; \tag{A16b}$$

$$\mathcal{S}_r^{\star(1)} \Big|_{jk} = \int_{\Omega} \mathbf{e}_{\mathbf{y}} \left(\mathbf{b}_k^{\star(1)} \right) : \mathbf{C} : \mathbf{e}_{\mathbf{y}} \left(\mathbf{b}_j^{\star(1)} \right) d\Omega_{\mathbf{y}}. \tag{A16c}$$

These lead to the relation in eq. (16) after scaling:

$$\mathcal{S}_t = \mathcal{S}_t^{\star} + \langle \mathbf{a}^{\star} \rangle; \qquad \mathcal{S}_c = \mathcal{S}_c^{\star} + \langle \mathbf{b}^{\star} \rangle; \tag{A17a}$$

$$\mathcal{S}_c' = \mathcal{S}_c^{\star}; \qquad \mathcal{S}_r = \mathcal{S}_r^{\star}. \tag{A17b}$$